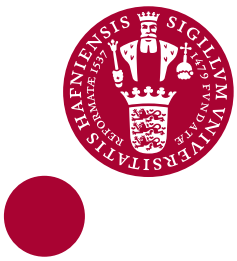

Geodynamic implications of synchronous norite and TTG formation in the 3 Ga Maniitsoq Norite Belt, West Greenland

Waterton, Pedro; Hyde, William Robert; Tusch, Jonas; Hollis, Julie A.; Kirkland, Christopher L.; Kinney, Carson; Yakymchuk, Chris; Gardiner, Nicholas J; Zakharov, David; Olierook, Hugo K.; Lightfoot, Peter C.; Szilas, Kristoffer

Published in:
Frontiers in Earth Science

DOI:
10.3389/feart.2020.562062

Publication date:
2020

Document version
Publisher's PDF, also known as Version of record

frontiers in Earth Science

ORIGINAL RESEARCH
published: 22 September 2020
doi: 10.3389/feart.2020.562062

Geodynamic Implications of Synchronous Norite and TTG Formation in the 3 Ga Maniitsoq Norite Belt, West Greenland

*Pedro Waterton[1], William R. Hyde[1], Jonas Tusch[2], Julie A. Hollis[3], Christopher L. Kirkland[4], Carson Kinney[5], Chris Yakymchuk[5], Nicholas J. Gardiner[6], David Zakharov[7], Hugo K. H. Olierook[4], Peter C. Lightfoot[8] and Kristoffer Szilas[1]**

[1] Department of Geosciences and Natural Resource Management, University of Copenhagen, Copenhagen, Denmark, [2] Institut für Geologie und Mineralogie, Universität zu Köln, Köln, Germany, [3] Department of Geology, Ministry of Mineral Resources, Government of Greenland, Nuuk, Greenland, [4] Centre for Exploration Targeting, Curtin Node, School of Earth and Planetary Sciences, Curtin University, Perth, WA, Australia, [5] Department of Earth and Environmental Sciences, Centre for Environmental and Information Technology (EIT), University of Waterloo, Waterloo, ON, Canada, [6] School of Earth and Environmental Sciences, Irvine Building, University of St. Andrews, St. Andrews, United Kingdom, [7] Institute of Earth Sciences, University of Lausanne, Lausanne, Switzerland, [8] North American Nickel Inc., Toronto, ON, Canada

OPEN ACCESS

Edited by:
Jean-Louis Vigneresse, Université de Lorraine, France

Reviewed by:
Oscar Laurent, UMR5563 Géosciences Environnement Toulouse (GET), France
Attilio Sulli, University of Palermo, Italy

***Correspondence:**
Kristoffer Szilas
krsz@ign.ku.dk

Specialty section:
This article was submitted to Geochemistry, a section of the journal Frontiers in Earth Science

Received: *14 May 2020*
Accepted: *25 August 2020*
Published: *22 September 2020*

Citation:
Waterton P, Hyde WR, Tusch J, Hollis JA, Kirkland CL, Kinney C, Yakymchuk C, Gardiner NJ, Zakharov D, Olierook HKH, Lightfoot PC and Szilas K (2020) Geodynamic Implications of Synchronous Norite and TTG Formation in the 3 Ga Maniitsoq Norite Belt, West Greenland. Front. Earth Sci. 8:562062. doi: 10.3389/feart.2020.562062

We present new data for the ~3.0 Ga Maniitsoq Norite Belt of the Akia Terrane, West Greenland, with the aim of understanding its petrogenesis. The Maniitsoq Norite Belt is hosted in regional tonalite-trondhjemite-granodiorite (TTG) and dioritic orthogneisses, intruded by later sheets of TTG and granite pegmatites, and comprises two main rock types: plagioclase-rich "norites" and pyroxene-rich "melanorites". Both norites and melanorites have high SiO_2 contents (52–60 wt% SiO_2), high bulk rock Mg# (0.57–0.83), and low TiO_2 contents (0.1–0.7 wt%). Their trace element patterns are defined by depleted heavy Rare-Earth elements, highly enriched light Rare-Earth elements, negative anomalies in Nb, Ta, and Ti, and variable anomalies in Zr, Hf, and Eu. New zircon U-Pb geochronology data and previously published ages establish an emplacement age of 3,013 ± 1 Ma for the majority of the Maniitsoq Norite Belt, with magmatism continuing until 3,001 ± 3 Ma. This ~12 Myr period of norite magmatism is coeval with an ongoing period of TTG production in the Akia Terrane. Norite Belt emplacement was closely followed by high temperature, low pressure granulite-facies metamorphism at ~800°C and <9 kbar. These conditions imply high temperature gradients (>900°C/GPa) and that the norite magmas were emplaced into thin crust and lithosphere. Compositions of the norites and melanorites can be explained by derivation from a single mafic parental melt (~13 wt% MgO), with the norites predominantly accumulating plagioclase and the melanorites predominantly accumulating pyroxene. Evidence from field relationships, the presence of xenocrystic zircon, major element compositions and combined trace element and Hf-isotope modelling suggests the norites were contaminated by assimilation of ~20–30% continental TTG crust. Geochemical and Hf-Nd isotopic constraints indicate that the norite mantle source was depleted, and that this depletion occurred significantly before

the emplacement of the norite magmas. Contemporaneous production of both TTGs and norite, their emplacement in thin crust, and the rapid transition to high temperature, low pressure granulite-facies metamorphism is best explained by their formation in an ultra-hot orogeny. Formation of norites in this setting may be restricted to >2.7 Ga, when geothermal gradients were higher on Earth.

Keywords: norite, crustal contamination, tonalite-trondhjemite-granodiorite and tonalite-trondhjemite-granodiorite-like gneisses, Nd isotope, Hf isotope, zircon U-Pb dating, granulite and amphibolite facies, ultra-hot orogen

INTRODUCTION

Norites are found in a range of settings on Earth, from oceanic crust (Nguyen et al., 2018) and ophiolites (Jaques, 1981), to layered mafic intrusions, such as the Bushveld Complex (Davies et al., 1980) and Stillwater Complex (Longhi et al., 1983), to impact melt sheets, such as the Sudbury Complex (Lightfoot, 2017). Of particular interest to investigations of the secular evolution of the Earth, is the observation of abundant intracratonic norites with "boninitic" affinities in the period from ~2.7 to ~2.0 Ga (Hall and Hughes, 1993; Srivastava, 2008; Pearce and Reagan, 2019). These appear to form part of a series of temporally restricted magmas, falling between the widespread occurrence of komatiite from ~3.5 to ~2.5 Ga (Arndt et al., 2008; Condie and O'Neill, 2010), and the appearance of the AMCG (anorthosite, mangerite, charnockite and rapakivi-granite) suite between ~1.8 and 1.0 Ga (Ashwal, 2010; Cawood and Hawkesworth, 2014; He et al., 2019). These temporal changes in magmatic style may have important implications for changes in tectonic regime and crustal growth through Earth history, and call into question the principle of uniformitarianism (Lyell, 1830; Hall and Hughes, 1993).

There has been considerable debate as to whether the ~2.7–2.0 Ga intracratonic noritic intrusions reflect "boninite-like" processes of re-melting of previously depleted and metasomatised mantle (Hall and Hughes, 1987; Smithies et al., 2004; Srivastava, 2008), or alternatively "siliceous high magnesium basalt-like" (SHMB) processes of severe crustal contamination of an ultramafic melt (Barnes, 1989; Bridgwater et al., 1995; Järvinen et al., 2019; Pearce and Reagan, 2019; Mansur and Barnes, 2020). Understanding if one or both of these processes were dominant in producing the ~2.7–2.0 Ga noritic suite is important for understanding the tectonic regime(s) that globally produced these norites. For example, a boninite-like origin might reflect the initiation of plate tectonics in this period (Condie, 2018), whereas an SHMB-like origin might suggest that the crustal conditions and the style of mantle derived magmas were favourable to the production of norites through crustal contamination during this time (Hall and Hughes, 1993).

Despite significant interest in the ~2.7–2.0 Ga noritic suite, there are few documented occurrences of "boninite-like" noritic rocks older than 2.7 Ga. In this regard, the exposed North Atlantic Craton in West Greenland may be unusual, with norites reported in the ~3 Ga Maniitsoq Norite Belt and associated "diorite" of the Fiskefjord region (Garde, 1991; Garde et al., 2013; Ravenelle et al., 2017), the ~3 Ga Amikoq Complex (Aarestrup et al. in press), and ~3.4 Ga noritic dykes in the Isua region (Nielsen et al., 2002). In this study, we present new field observations, petrography, geochemical and isotopic data, and phase equilibrium modelling for the ~3 Ga Maniitsoq Norite Belt, with the aim of understanding its petrogenesis. We critically assess the close relationship between norite and tonalite-trondhjemite-granodiorite (TTG) formation in the Maniitsoq region, and examine the role of crustal contamination in the formation of the Maniitsoq Norite Belt. Finally, we present a tectonic model for the formation of the Maniitsoq Norite Belt, and compare this to existing models for younger norites.

GEOLOGICAL SETTING, FIELD OBSERVATIONS, AND SAMPLES

The Akia Terrane

The Maniitsoq Norite Belt is located within the Mesoarchaean Akia Terrane of the North Atlantic Craton, West Greenland. The Akia Terrane is bounded to the southeast by the Eo- to Neoarchaean tectonostratigraphic terranes of the Nuuk region (Friend and Nutman, 2019). Its northern boundary is marked by the recently recognised <2.9 Ga Alanngua Complex (Steenfelt et al., in review), which separates the Akia Terrane from the proposed Tuno terrane (Friend and Nutman, 1994; Nutman et al., 2004; Yi et al., 2014). The Akia Terrane is dominated by orthogneisses recording two major crust forming events: an early event represented by ~3,240–3,180 Ma Nordlandet dioritic gneisses, and a later event comprising ~3,050–2,990 Ma gneisses with predominantly TTG and dioritic compositions (Garde, 1997; Garde et al., 2000; Gardiner et al., 2019). These TTG gneisses contain enclaves of supracrustal rocks, dominated by tholeiitic and calc-alkaline amphibolites with a depositional age of 3,071 ± 1 Ma (Garde, 1997, 2007; Szilas et al., 2017; Gardiner et al., 2019), and enclaves of mafic-ultramafic intrusive complexes, which predate the TTGs (Szilas et al., 2015, Szilas et al., 2018). Despite Mesoarchaean igneous ages throughout, Hf isotopic data from zircons indicate the presence of a mafic Eoarchaean precursor to the Akia Terrane (Gardiner et al., 2019).

The formation of voluminous TTGs immediately predates, or is contemporaneous with, extensive regional high

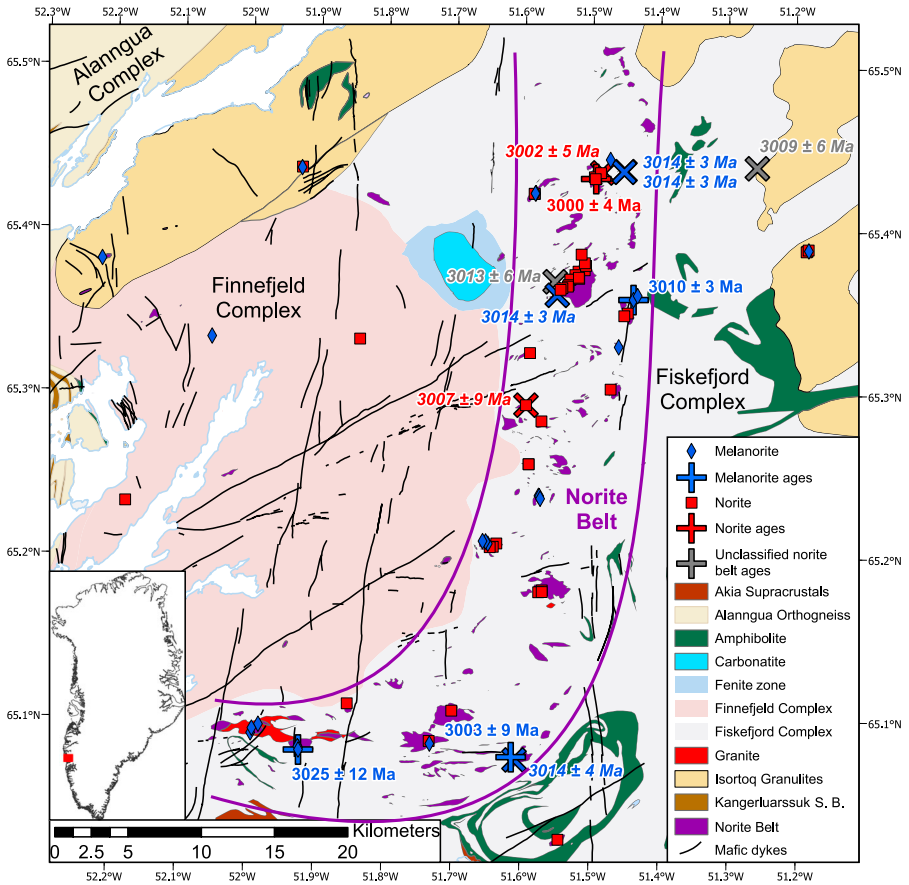

FIGURE 1 | Geological map of the Maniitsoq Norite Belt, showing location of all samples analysed for this study. Norite belt U-Pb zircon ages from this study (straight crosses, regular text) and previous work (diagonal crosses, italics; Ravenelle et al., 2017; Gardiner et al., 2019; Aarestrup et al., in press) are shown adjacent to their sample locations. Ages are colour coded by whether the sample was classed as norite (red), melanorite (blue), or unclassified (grey). Approximate extent of the Maniitsoq Norite Belt is delineated by purple curves. S. B. = Supracrustal Belt. Location of map within Greenland shown in inset.

temperature, low pressure metamorphism across the Akia Terrane between ~3,010 and 2,980 Ma (Riciputi et al., 1990; Friend and Nutman, 1994; Garde et al., 2000; Yakymchuk et al., 2020). Metamorphic grades reached granulite-facies conditions of >800°C at <0.9 GPa across much of the Akia Terrane (Yakymchuk et al., 2020), though the easternmost part of the terrane may have only experienced upper amphibolite-facies conditions (Garde, 1997). This high temperature metamorphism was followed by widespread but variable amphibolite-facies retrogression (Garde, 1997), though the timing of this retrogression is poorly constrained. Granulite facies metamorphism is also recorded at ~2.86–2.70 Ga in the Alanngua Complex, at the northern margin of the Akia Terrane, which may record the juxtaposition of the Tuno and Akia terranes (Kirkland et al., 2018; Steenfelt et al., in review). This event is marked in the Akia Terrane by the widespread intrusion of granitic pegmatitic dykes at ~2,720 Ma (Friend et al., 1996; Gardiner et al., 2019). A shared Neoarchaean metamorphic history between the Akia and its bounding terranes (Friend and Nutman, 2005; Kirkland et al., 2018), indicates that their juxtaposition was complete by at least 2.72 Ga. Further amphibolite- to granulite-facies metamorphism is recorded in the Alanngua Complex at 2.56 Ga (Dyck et al., 2015; Steenfelt et al., in review; Yakymchuk et al., in review) and the Akia terrane at 2.54 Ga (Kirkland et al., 2020). This coincides with minor granite intrusions in the northern Akia Terrane (Gardiner et al., 2019) and the intrusion of the Qôrqut Granite Complex along the southern margin of the Akia Terrane (Nutman et al., 2010; Næraa et al., 2014), and has been associated with final cratonisation of the North Atlantic Craton (Yakymchuk et al., in review).

The Maniitsoq Norite Belt

The Maniitsoq Norite Belt forms an approximately 75 km by 15 km 'J'-shaped belt of norite bodies included within ~3.0 Ga regional TTGs and dioritic gneisses of the Akia Terrane (Secher, 1983, Secher, 2001; Garde et al., 2012, Garde et al., 2013; Ravenelle et al., 2017) (**Figure 1**). The Norite Belt predominantly outcrops within TTG-dominated orthogneisses of the Fiskefjord Complex, and is spatially associated with the southern and eastern edges of the dioritic and TTG orthogneisses

of the Finnefjeld Complex (Steenfelt et al., in review). Garde et al. (2012) and (2013) suggested a genetic link to the "post-kinematic diorites" of the Fiskefjord region (Garde, 1991), which along with recently discovered norite outcrops to the north of the main norite belt (Ravenelle et al., 2017) imply norite magmatism occurred over length scales >100 km. Norite bodies range in size from kilometre-scale (e.g., the 8 km^2 Fossilik body; Ravenelle et al., 2017) to meter-scale pods (Garde et al., 2013). Unlike other mafic–ultramafic complexes further south in the Akia Terrane (Garde, 1997; Szilas et al., 2015), the norites are not closely associated with other ultramafic cumulates. Previously geochronological studies suggest the norites formed between ~3,014 and ~3,002 Ma (Ravenelle et al., 2017), or between ~2,976 and ~3,017 Ma by correlation with the Fiskefjord diorites (Garde, 1991; Garde et al., 2000; Scherstén and Garde, 2013).

A wide variety of compositions have been reported in the norite belt, ranging from quartz diorite, through norite, to pyroxenite (Garde et al., 2013; Ravenelle et al., 2017). However, despite this range, the rocks can be broadly described as high in MgO, Cr, and Ni, with relatively high SiO_2, and consistent trace element patterns across the range of compositions (Garde et al., 2012). The norite belt intrusions host significant nickel-sulphide mineralisation, both as primary magmatic sulphide and as secondary sulphides remobilised during high-grade metamorphism. Sulphide mineralisation is predominantly concentrated in the highest MgO norites and pyroxenites, and is the subject of ongoing exploration work by North American Nickel (Ravenelle et al., 2017).

Field Observations and Sampling

Fieldwork was conducted in the Maniitsoq region of the Akia Terrane in 2016 and 2017. Two major rock types are distinguishable in the norite belt based on field observations. The first, which constitutes a majority (~60–80%) of the exposed norite belt comprises medium- to coarse-grained plagioclase-rich rock with a granitoid-like texture and blueish/grey plagioclase. The presence of both clinopyroxene and orthopyroxene, means these should strictly be termed "gabbronorites" (Le Maitre et al., 2002). However, we retain the use of the term norite to describe these rocks for simplicity and continuity with previous studies describing the "norite" belt (Garde et al., 2012, Garde et al., 2013; Ravenelle et al., 2017). These norites are generally massive and mineralogically homogenous, forming rounded friable grey outcrops (**Figure 2A**). They occasionally contain enclaves of layered amphibolite (**Figure 2B**), and therefore post-date the earliest mafic crust in the region.

The remainder (~20–40%) of the norite belt comprises orthopyroxene-rich rocks, which we term "melanorites" (pyroxenites and norites of Ravenelle et al., 2017) to distinguish them from the plagioclase-rich norites. These are typically brown in colour due to their orthopyroxene-rich nature and weather to form rounded outcrops with blocky protrusions (**Figure 2C**). Some have a "spotted" appearance due to the presence of coarse orthopyroxene-rich and plagioclase-rich zones (**Figure 2D**), which correspond to the "leopard norites" of Ravenelle et al. (2017) and have been described as "proto-orbicular" by Garde et al. (2012).

Both norites and melanorites may be observed in the same body, particularly in the larger bodies. In these larger bodies, such as the Fossilik intrusion, norites are found towards the palaeo-top of the intrusion, whereas melanorites are found towards the base (Ravenelle et al., 2017). Contacts between the norites and melanorites are frequently obscured by deformation or erosion but appear to be transitional where exposed. Furthermore, rare examples of igneous banding (**Figure 2E**; Secher, 1983) generated by variations in the proportions of plagioclase and pyroxene appear to represent alternating norite and melanorite compositions. We therefore interpret the norites and melanorites as part of the same magmatic suite.

Both types of norite are intruded by two different types of felsic magmas. The first are TTG sheets ranging in size from a few centimetres to a few metres (**Figure 2F**). These are often internally sheared, suggesting that the TTGs were incompetent relative to the norites during later deformation. The second are late (undeformed) granite pegmatites up to 20 m wide (**Figure 2G**), which cut the TTG sheets and extend into the regional TTG orthogneiss. Adjacent to the granites, the norites are altered to a more cohesive amphibolite with a "gabbroic" appearance (**Figure 2G**). The melanorites, by contrast, are altered to green amphibolite with plagioclase taking on a "snowflake"-like appearance.

Field evidence for the relative timing of norite and TTG formation is equivocal. Contacts to their host TTG gneisses are generally tectonised, obscuring whether the norites are intrusions into the regional TTG gneisses, or enclaves included within the gneisses. The norites were previously interpreted as "post-kinematic" intrusive plugs which post-date the regional TTG gneisses (Garde et al., 2012, Garde et al., 2013), and many of the larger norite bodies may fit this interpretation. However, it is difficult to reconcile the smallest metre-scale norite bodies with this model, and they may instead represent enclaves intruded by the TTGs or tectonically emplaced slivers from larger norite bodies. No evidence was found of reported 3.0 Ga dykes related to the norite belt (Garde et al., 2012, Garde et al., 2013), though Palaeoproterozoic noritic dykes are common in this area (Berthelsen and Bridgwater, 1960; Hall and Hughes, 1987; Nutman et al., 1995). Tonalitic sheets cross-cutting the norites appear continuous with the regional orthogneisses, suggesting that at least some TTGs post-date norite intrusion. However, a hybridised contact zone between norite and TTG at one locality (**Figure 2H**), and previous reports of gneiss xenoliths included in norite (Secher, 1983), indicate that norite intrusion post-dated the emplacement and deformation of at least some TTGs. To summarise, the field evidence provides no systematic relative emplacement sequence between the norites and TTGs; locally, norites appear to both precede and post-date TTG emplacement.

There is abundant evidence that the norites are not post-kinematic, and predate the end of deformation in the Akia Terrane, including: isoclinal folding and boudinage of the norite bodies, complex folding of contacts between the norites and their host orthogneisses, internal shearing of TTG sheets that

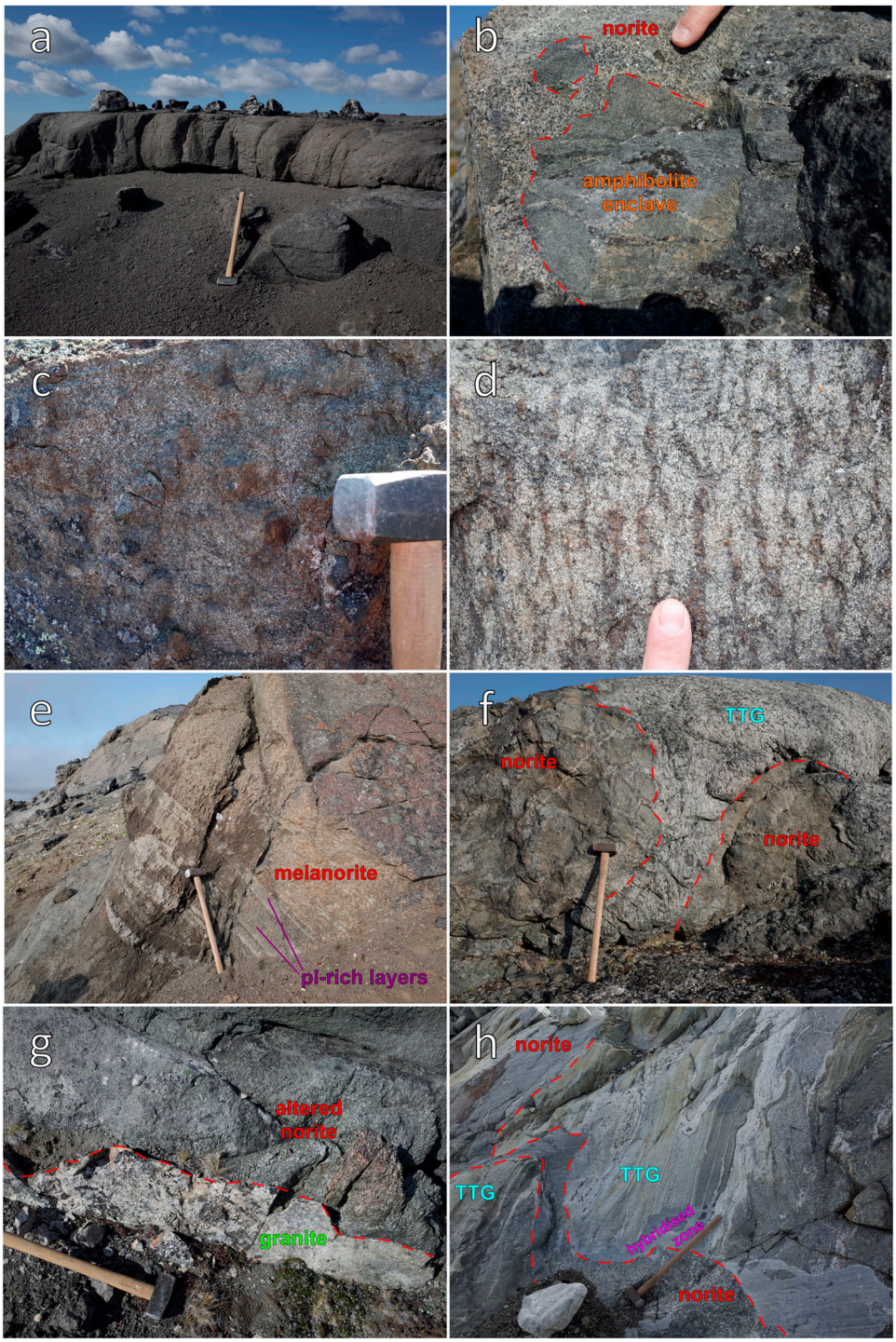

FIGURE 2 | Field photos of the Maniitsoq Norite Belt. **(A)** Typical outcrop of homogenous grey norite (sample 815). **(B)** Amphibolite (sample 820) included within norite (sample 821). **(C)** Close up of a melanorite outcrop, with brown orthopyroxene and white plagioclase visible, and blocky weathering (sample 804). **(D)** Close up of spotted norite texture with plagioclase- and orthopyroxene-rich zones in melanorite (sample 875). **(E)** Melanorite outcrop with pale plagioclase-rich (pl-rich) igneous layering (sample 1,258). **(F)** Pale tonalitic sheet (sample 1,256) intruding darker coloured norite (sample 1,257). **(G)** Thin granite pegmatite sheet (sample 814) intruding norite. Norite is green with a "gabbroic" texture adjacent to sheet. **(H)** Enclave of banded TTG orthogneiss (sample 1,260) included in norite, suggesting norites post-date at least some of the regional TTGs.

cross-cut the norites, the occurrence of a lineated tectonic fabric in some norites that is parallel to regional tectonic fabrics in the host orthogneisses, and the presence of mylonite sheets in the norites (Ravenelle et al., 2017). In contrast to other metabasites in the Akia Terrane (Yakymchuk et al., 2020), the norites do not show evidence of anatexis.

A large number of samples identified as norites, gabbros, or diorites in the field were collected. Of these, 69 could reliably be identified as "norite belt" samples: the majority were collected from the main norite belt (Garde et al., 2012; Ravenelle et al., 2017); a minority that were collected elsewhere but were petrologically and geochemically indistinguishable from the rocks of the norite belt. Of these, some are found within and to the north of the Finnefjeld Orthogneiss Complex, while others occur to the east and south of the main norite belt (**Figure 1**). The studied samples are mostly unmineralised. In addition, a large number of amphibolites included in the regional TTGs and/or norites, and a number of felsic sheets crosscutting the norite belt, were sampled.

PETROGRAPHY

Norites

The norites are dominated by coarse-grained anhedral plagioclase, interspersed with aggregates of mafic material. Samples identified as fresh norites in the field have granoblastic textures with an assemblage of plagioclase + orthopyroxene + clinopyroxene + hornblende ± biotite ± quartz, corresponding to a largely dry granulite-facies metamorphic assemblage (**Figures 3A,B**; see **Supplementary Material** for additional examples of granoblastic textures). Accessory minerals include magnetite, ilmenite, and Fe-Ni sulphides. No igneous textures are preserved. Visually estimated plagioclase contents range from 60–85 vol%, and orthopyroxene contents (10–15 vol%) are generally slightly higher than or equal to clinopyroxene contents (5–15 vol%). Orthopyroxene and clinopyroxene are subhedral to anhedral; clinopyroxene is often twinned. Both pyroxenes commonly show epitaxial replacement predominantly by hornblende and rarely other amphiboles (actinolite-tremolite), forming lamellae and/or amorphous inclusions within the pyroxenes. In rare cases, these lamellae comprise pyroxene (e.g., orthopyroxene lamellae in clinopyroxene; **Figure 3C**). Hornblende also occurs as distinct grains. Samples show no obvious mineral alignment, though some evidence of deformation is visible in deformed plagioclase twins and bent cleavages in orthopyroxene.

In samples collected adjacent to intruding granite pegmatites, and in portions of samples adjacent to veins, the granulite-facies assemblage is retrogressed to an amphibolite-facies assemblage of plagioclase + hornblende + biotite ± quartz (**Figure 3D**). Plagioclase retains a granoblastic texture in the retrogressed norite. However, the ratio of plagioclase to mafic minerals is lower in the retrogressed norites, and plagioclase grain size tends to be smaller. The mafic portions of the retrogressed norites show a fine-grained interlocking texture of biotite and amphibole. Biotite contents are higher in retrogressed samples. Coexisting retrogressed and non-retrogressed assemblages and textures are visible at the scale of a single thin section in some samples.

Melanorites

The melanorites comprise an assemblage of orthopyroxene + hornblende + plagioclase ± clinopyroxene ± minor biotite (**Figures 3E,F**), which we interpret as a granulite-facies metamorphic mineral assemblage. Proportions of these minerals vary strongly. Some samples are almost orthopyroxenites (up to 75 vol% orthopyroxene; **Figure 3G**), with hornblende and very small amounts of plagioclase and clinopyroxene (<5 vol%). Others range to relatively plagioclase rich (up to 45 vol%) or clinopyroxene rich (up to 30 vol%) compositions. Accessory minerals include magnetite, ilmenite, rutile, and Fe-Ni sulphides; sulphides are frequently associated with Fe-oxides and alteration along veins. Textures are generally granoblastic but rarely appear cumulate-like in some orthopyroxene-rich samples. Where igneous textures are still identifiable, former ~30° melt-solid dihedral angles (Holness, 2006) systematically show textural equilibration to 120° joints (**Figure 3F**). Spotted norite samples (**Figure 2D**) show variations between orthopyroxene-rich zones and plagioclase-rich zones. Plagioclase-rich zones still contain aggregates of mafic minerals, albeit in lower proportions, which have previously been interpreted as proto-orbicular textures, indicating rapid crystallisation (Garde, 1991; Garde et al., 2012, Garde et al., 2013). However, although the broad variations between plagioclase- and orthopyroxene-rich zones may reflect primary igneous features, the present textures are entirely metamorphic and are not indicators of crystallisation rate. Both orthopyroxene and clinopyroxene are subhedral to anhedral and have a ragged appearance, with bent cleavages and epitaxial replacement by amphibole. Similar to the norites, hornblende is found as both large distinct grains and replacing orthopyroxene and clinopyroxene. Biotite contents tend to be higher in samples with higher amphibole and lower orthopyroxene contents, and is absent in some samples.

Some melanorites show patchy retrogression, with areas showing a fine-grained interlocking texture of acicular amphiboles (**Figure 3H**) interspersed within the typical granulite-facies assemblage described above. Small relicts of orthopyroxene are visible in these retrogressed areas. As with the norites, this retrogression is associated with a reduction in plagioclase mode, with the complete loss of plagioclase in some cases.

METHODS

Detailed analytical methods for mineral analyses by electron probe micro-analysis (EPMA); bulk rock major, trace, and platinum group elements (PGEs), ^{147}Sm-^{143}Nd and ^{176}Lu-^{176}Hf isotopic analyses, oxygen isotope analyses, U-Pb zircon geochronology, and phase equilibrium modelling are given in the **Supplementary Material**. Bulk-rock major and trace element

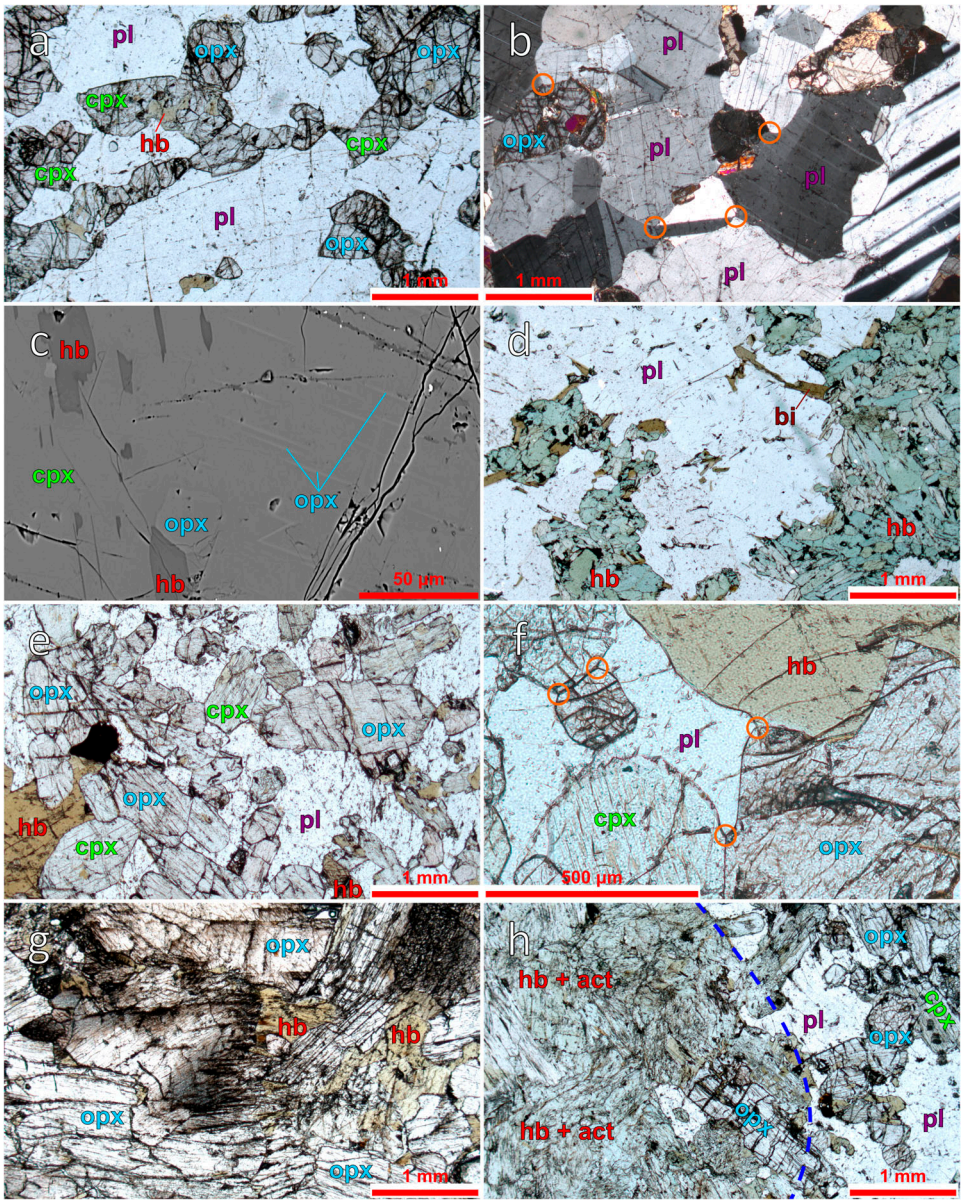

FIGURE 3 | Photomicrographs and back-scattered electron (BSE) images of norite belt samples; photomicrographs are plane-polarised light unless stated otherwise. **(A)** Typical norite with granulite-facies assemblage of orthopyroxene (opx), clinopyroxene (cpx), plagioclase (pl), and hornblende (hb). **(B)** Cross-polarised light photomicrograph of granoblastic-textured plagioclase-rich norite, orange circles highlight well-equilibrated grain boundary triple junctions. **(C)** BSE image of lamellae and blocky inclusions of orthopyroxene and hornblende in a clinopyroxene grain. **(D)** Retrogressed norite from adjacent to an intrusive granite, showing an amphibolite-facies assemblage dominated by plagioclase and hornblende (hb), with minor biotite (bi). **(E)** Typical melanorite granulite-facies assemblage, note higher proportion of orthopyroxene compared to norite. **(F)** Typical melanorite showing textural equilibrium between major mineral phases, orange circles highlight well-equilibrated grain boundary triple junctions. Brown inclusions in clinopyroxene are hornblende. **(G)** Orthopyroxene rich melanorite, with minor hornblende. **(H)** Melanorite with patchy retrogression, blue dashed line divides retrogressed assemblage dominated by hornblende and actinolite (act), with minor plagioclase and relict orthopyroxene, from typical melanorite granulite assemblage.

compositions were determined for all samples at ALS Laboratories, but due to concerns over trace element data quality a subset of samples were reanalysed at Washington State University (WSU). The ALS major and minor element data is used for samples not reanalysed at WSU, but the majority of trace elements analysed by ALS are not used in this study (**Supplementary Material**).

RESULTS

Electron Probe Micro-Analysis Mineral Chemistry

Norites

Plagioclase compositions (**Figure 4**; **Supplementary Table S3**) range from An_{48}–An_{59} in samples dominated by granulite-facies

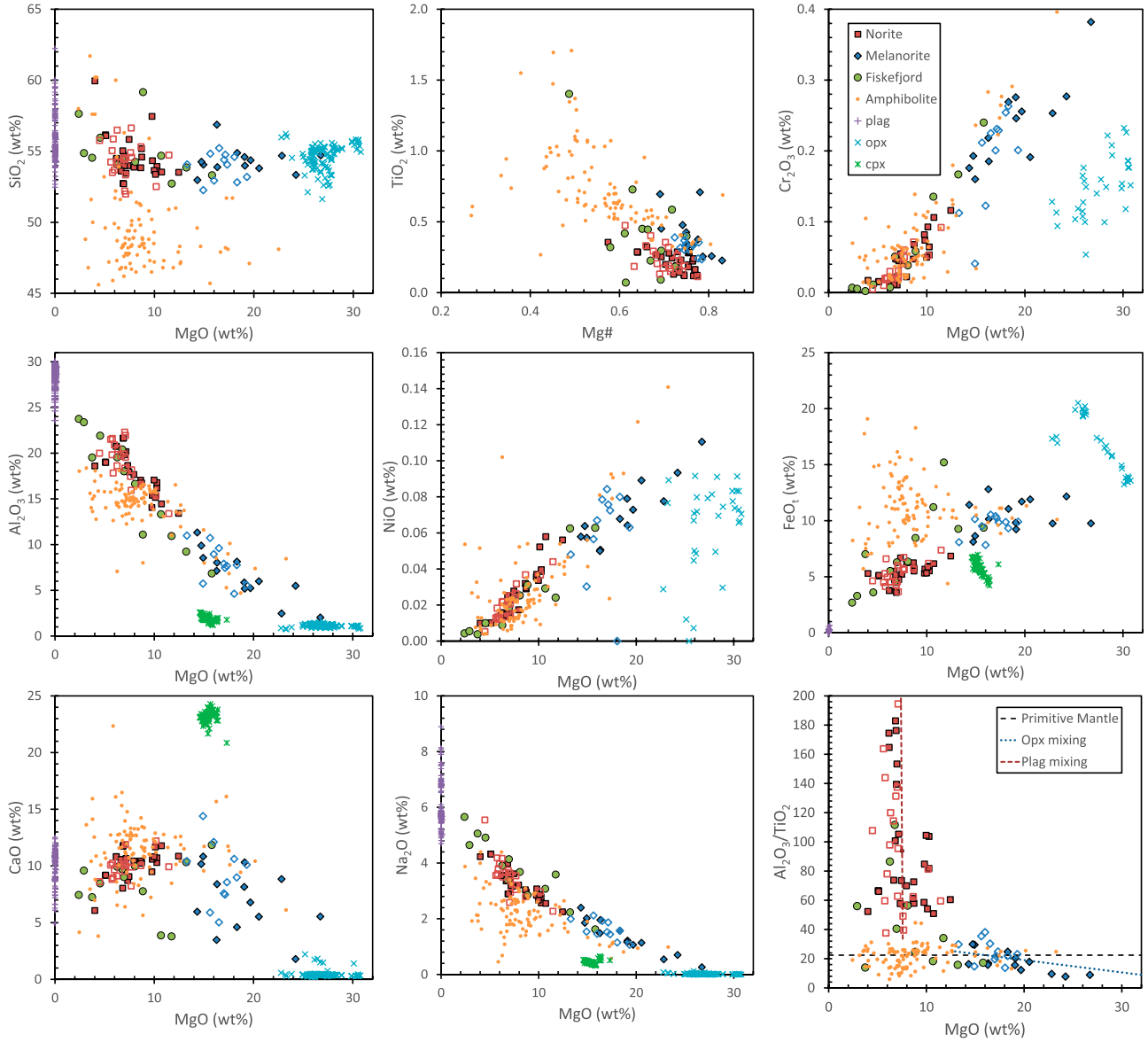

FIGURE 4 | Bulk rock major and minor element variations for norite belt samples. Solid symbols indicate WSU data, hollow symbols indicate ALS data. Norites and melanorites are compared to Akia Terrane amphibolites from the Maniitsoq region, and "post kinematic diorites" of the Fiskefjord region (Garde, 1991). Compositions of major mineral phases in norite and melanorite samples are also shown, compositions in norites and melanorites are very similar and not distinguished here. Clinopyroxene is omitted from some plots for clarity, and plagioclase is omitted from plots of elements with very low concentrations in plagioclase. "Opx mixing" and "Plag mixing" are mixing lines between the average melanorite bulk rock composition and the average orthopyroxene composition determined by EPMA, and the average norite composition and average plagioclase composition, respectively. Average plagioclase has $Al_2O_3/TiO_2 \approx 7{,}000$ and is not shown. Primitive mantle Al_2O_3/TiO_2 from Hofmann (1988).

assemblages (average An_{52}), and from An_{23}–An_{52} in retrogressed samples (average An_{45}). Plagioclase is unzoned, with consistent compositions in each sample compared to the variation between samples, even for samples showing both retrogressed and granulite-facies mafic mineral assemblages in individual thin sections. Strongly retrogressed samples, from near intrusive granites have the lowest An plagioclase. Both orthopyroxene and clinopyroxene and unzoned and show consistent compositions throughout, with overlapping compositions in granulite-facies and partially retrogressed samples; no pyroxene is preserved in the most retrogressed samples. Orthopyroxene has low Ca (<Wo_4, average Wo_1) and Mg# (Mg# = molar Mg/[Mg + Fe^{2+}]) from 0.67–0.77. Clinopyroxenes are diopsides, with high Ca (>Wo_{45}, average Wo_{47}) and slightly higher Mg# than the orthopyroxenes (Mg# 0.79–0.85). The vast majority of amphiboles analysed in the granulite-facies assemblage are magnesio- or magnesio-ferri-hornblendes (Hawthorne et al., 2012; Locock, 2014), including the majority of inclusions and

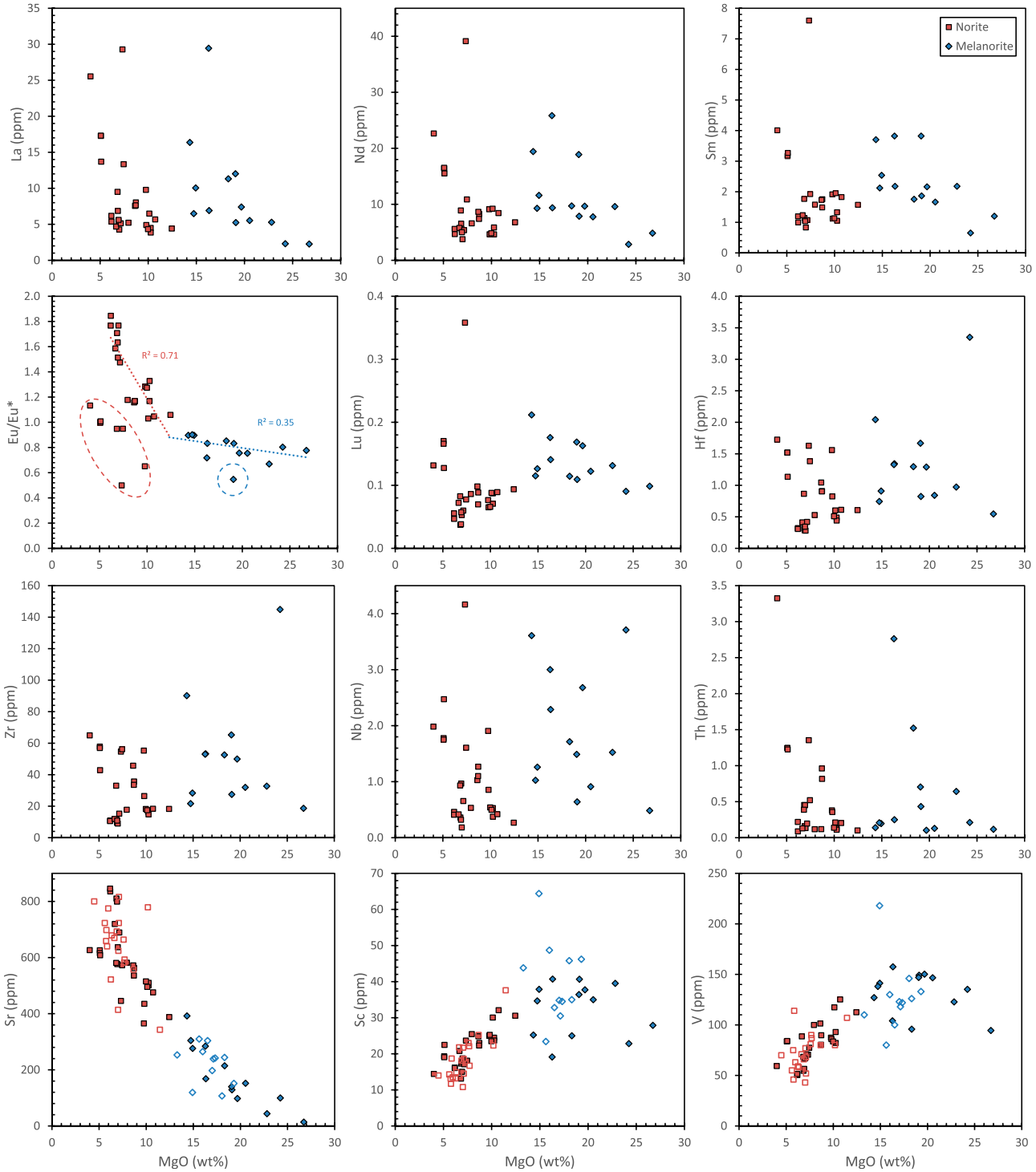

FIGURE 5 | Variation of selected trace elements in norite belt samples, plotted against MgO. Solid and hollow symbols refer to WSU and ALS data, respectively. Dashed lines in Eu/Eu* against MgO plot are regressions of selected data with R^2 values shown. Data in dashed circles were excluded from the regressions either because they showed signs of retrogression (melanorites) or evidence of having formed from more evolved melts (norites).

lamellae in the pyroxenes. The EPMA analyses also identified rare inclusions of actinolite-tremolite and rare examples of pyroxene inclusions and lamellae (**Figure 3B**). Retrogressed mafic assemblages contain both magnesio-ferri-hornblende and actinolite-tremolite, direct replacement of orthopyroxene by cummingtonite is also observed. Biotite in the granulite-facies assemblage tends to be Mg- and Ti-rich (Mg# 0.73–0.76, TiO_2 3.6–4.0 wt%), consistent with higher temperatures of equilibration

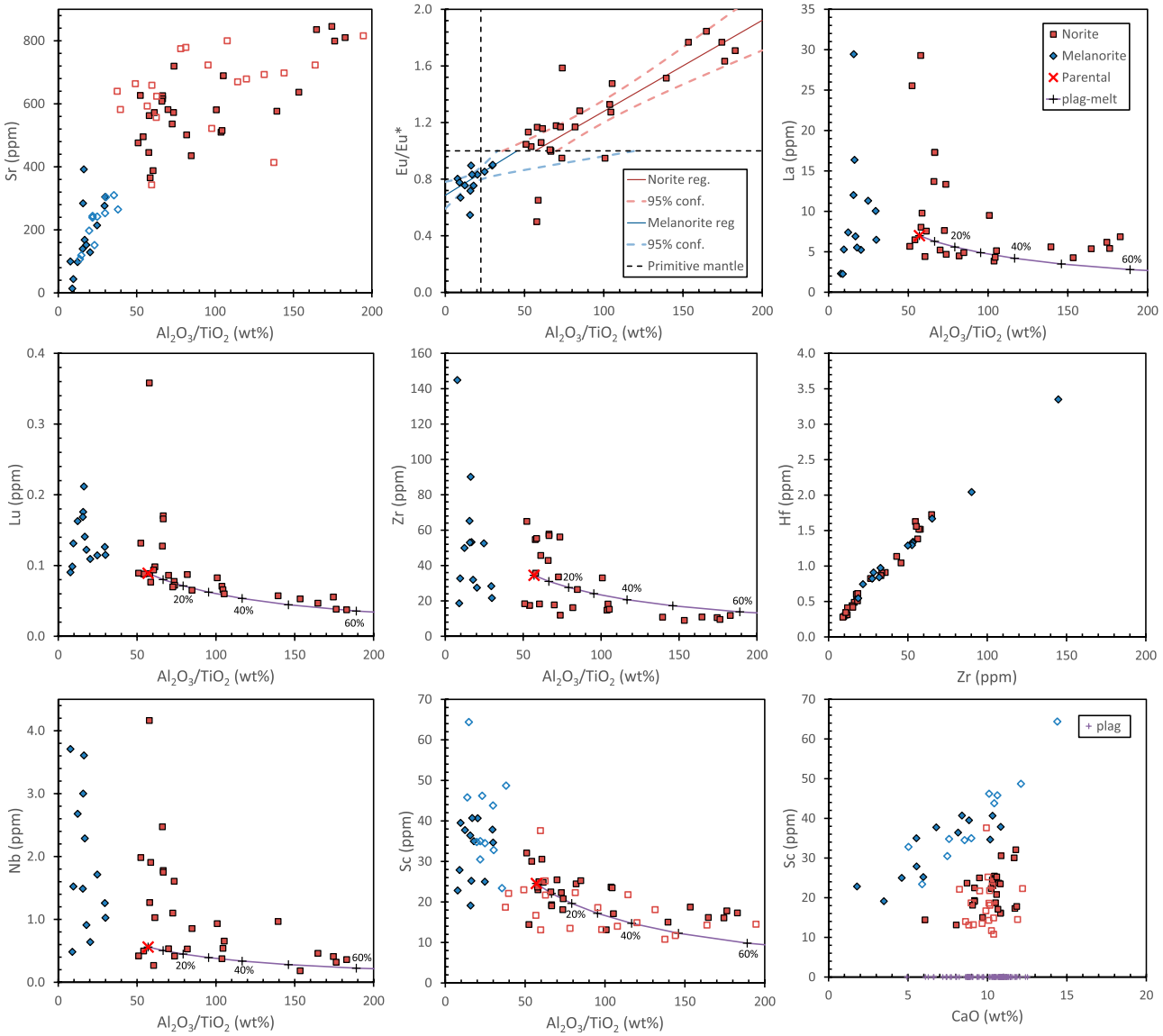

FIGURE 6 | Variation of selected trace elements in norite belt samples. Eu/Eu* plot shows regressions of norite and melanorite data (with 95% confidence limits about the regression) to assumed parental magma compositions with Eu/Eu* = 1, primitive mantle Al_2O_3/TiO_2 (Hofmann, 1988) is shown for comparison. "Parental" indicates the approximate parental magma composition for the norites calculated at Eu/Eu* = 1. "plag-melt" curves are mixing relationships between this parental melt and plagioclase compositions, indicating plagioclase accumulation. Lutetium, La, Zr, Nb, and Sc are incompatible in plagioclase (Aigner-Torres et al., 2007) and assumed to have concentrations of zero. Crosses are 10% increments of plagioclase fraction in the mixture (by weight), some increments are labelled with percentage symbols. Range of plagioclase CaO contents is show in the Sc plot, at an assumed Sc content of 0 ppm. Solid and hollow symbols refer to WSU and ALS data, respectively.

(Patiño Douce, 1993) than biotite in the retrogressed assemblages (Mg# 0.66–0.72, TiO_2 1.5–3.5 wt%).

Melanorites

Plagioclase compositions in the melanorites are also consistent within a given sample, though generally more Na-rich than the norites, regardless of the degree of retrogression. Plagioclase crystals are unzoned. Compositions range from An_{35}–An_{43}, with the most Na-rich plagioclase found in the most orthopyroxene rich/plagioclase poor sample. Orthopyroxene grains are unzoned with compositions varying from Mg# 0.69–0.80 with $<Wo_3$. Clinopyroxene grains are unzoned (where present), with compositions ranging from Mg# 0.83–0.87 generally with $>Wo_{45}$. Taken together with the norites, the clinopyroxene and orthopyroxene average Mg# strongly correlate with bulk rock Mg#, indicating equilibration with the bulk rock compositions during metamorphism (**Supplementary Material**). Amphiboles are dominantly

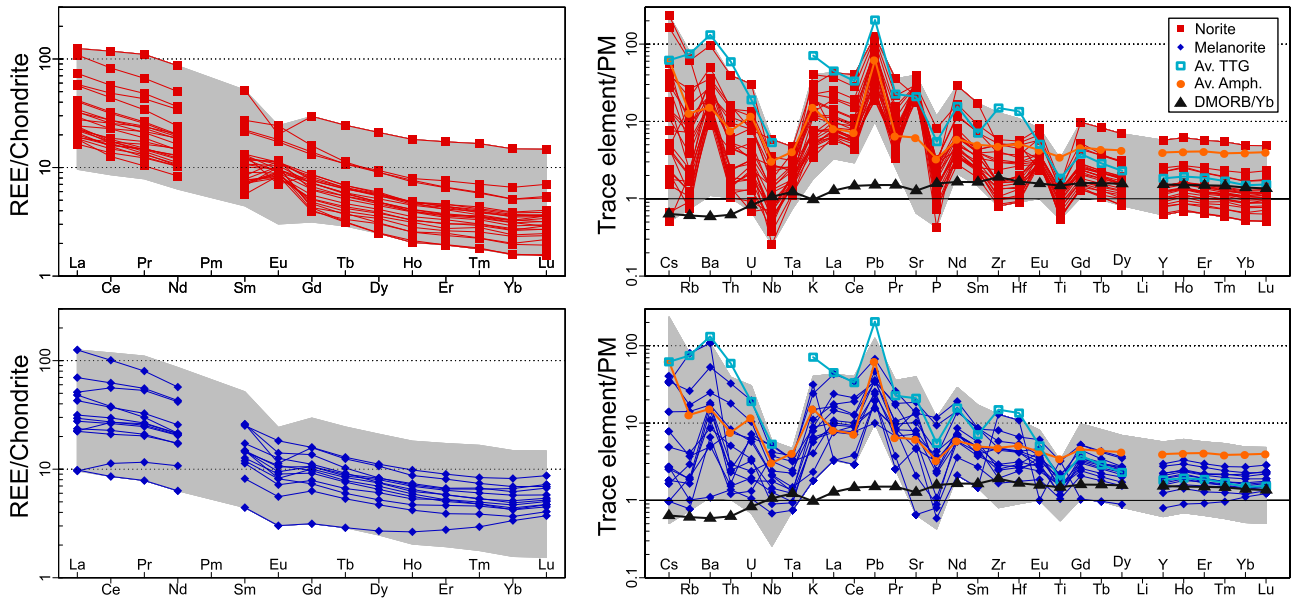

FIGURE 7 | Rare earth element and trace element spider plots for norite and melanorite samples. REE plots are normalised to chondrite (Anders and Grevesse, 1989), trace element plots to primitive mantle (PM; Sun and McDonough, 1989). Grey fields indicate total range of values from both groups for comparison. Also shown are the average trace element patterns for Maniitsoq amphibolites ("Av. amph."; n = 100; **Supplementary Table S1**), the average trace element composition of TTGs, felsic orthogneisses, and granites from the Maniitsoq region ("Av. TTG"; n = 147; Gardiner et al., 2019). The average depleted MORB composition of Gale et al. (2013), normalised to the average Yb content in norite belt samples, is shown for reference as a typical depleted mantle melt composition.

magnesio-ferri-hornblende and pargasite (Hawthorne et al., 2012; Locock, 2014), though tremolite-actinolite is more common than in the analysed norites and appears as an alteration product of hornblende. Replacement of orthopyroxene by cummingtonite is also more common than in the norites, particularly associated with veins and in retrogressed patches. One biotite analysed in a granulite-facies sample had an Mg# of 0.79, one biotite analysed in a retrogressed sample had an Mg# of 0.72. Some magnetites are Cr-rich, and may reflect alteration products of chromite.

Bulk-Rock Major and Trace Elements

Major Elements

Both norites and melanorites have similar SiO_2 contents (52–60 wt% SiO_2; **Figure 4**; **Supplementary Table S1**), which are high relative to amphibolites included in the regional TTG orthogneisses. Norites and melanorites have low TiO_2 (0.1–0.7 wt %) and high Mg# (0.57–0.83) relative to most amphibolites, though there is some overlap between the most mafic amphibolites and the melanorites. Data for a number of elements (Al_2O_3, CaO, FeO_t, Na_2O) form broad continuous trends between the norites and melanorites, with the melanorites having more mafic compositions and higher MgO, Cr_2O_3, and NiO. However, the melanorites have higher average Ti contents than the norites. Perhaps the most striking difference between the two groups is seen in their Al_2O_3/TiO_2 ratios, which are similar to or lower than primitive mantle values in the melanorites, but extend to extremely high Al_2O_3/TiO_2 at approximately constant MgO in the norites. Loss-on-ignition (LOI) values are low (typically <1 wt%) in both the norites and melanorites, though some retrogressed samples have LOI above 1 wt%. Compositions of "post-kinematic diorites" of the Fiskefjord region (Garde, 1991) are also plotted in **Figure 4**, and show similar compositions to the norites and the less mafic melanorites.

Trace Elements

Bulk rock trace element variations are plotted in **Figures 5–7**, and available in **Supplementary Table S1**. Rare-Earth elements (REE) are generally negatively correlated with MgO in the melanorites, with scatter increasing towards the light-REEs (LREE), and show no correlation with MgO in the norites. Heavy-REE (HREE) contents are generally higher in the melanorites than norites, though LREE contents broadly overlap between the two groups. However, when plotted against Al_2O_3/TiO_2, the norite REE data show two diverging trends: one towards decreasing or flat REE content with increasing Al_2O_3/TiO_2, another towards high REE contents at constant Al_2O_3/TiO_2. The latter trend is more pronounced in the LREEs than HREEs. High field strength elements (HFSE) show broad scatter in both groups of samples against MgO, but again follow similar (though more scattered) diverging trends in the norite samples when plotted against Al_2O_3/TiO_2. Strontium has a similar distribution against MgO to Al_2O_3, and is correlated with Al_2O_3/TiO_2. The norites generally show positive Eu anomalies ($Eu/Eu^* = 2 \times Eu_N/[Sm_N + Gd_N]$, "N" indicates primitive mantle normalised), whereas all melanorite samples show negative Eu anomalies. These anomalies are correlated with Al_2O_3/TiO_2, particularly in the norites. Scandium shows a scattered distribution against MgO, similar to CaO, and is correlated with CaO in the melanorites. Most large ion lithophile elements (LILE) show a high degree of scatter and are not shown.

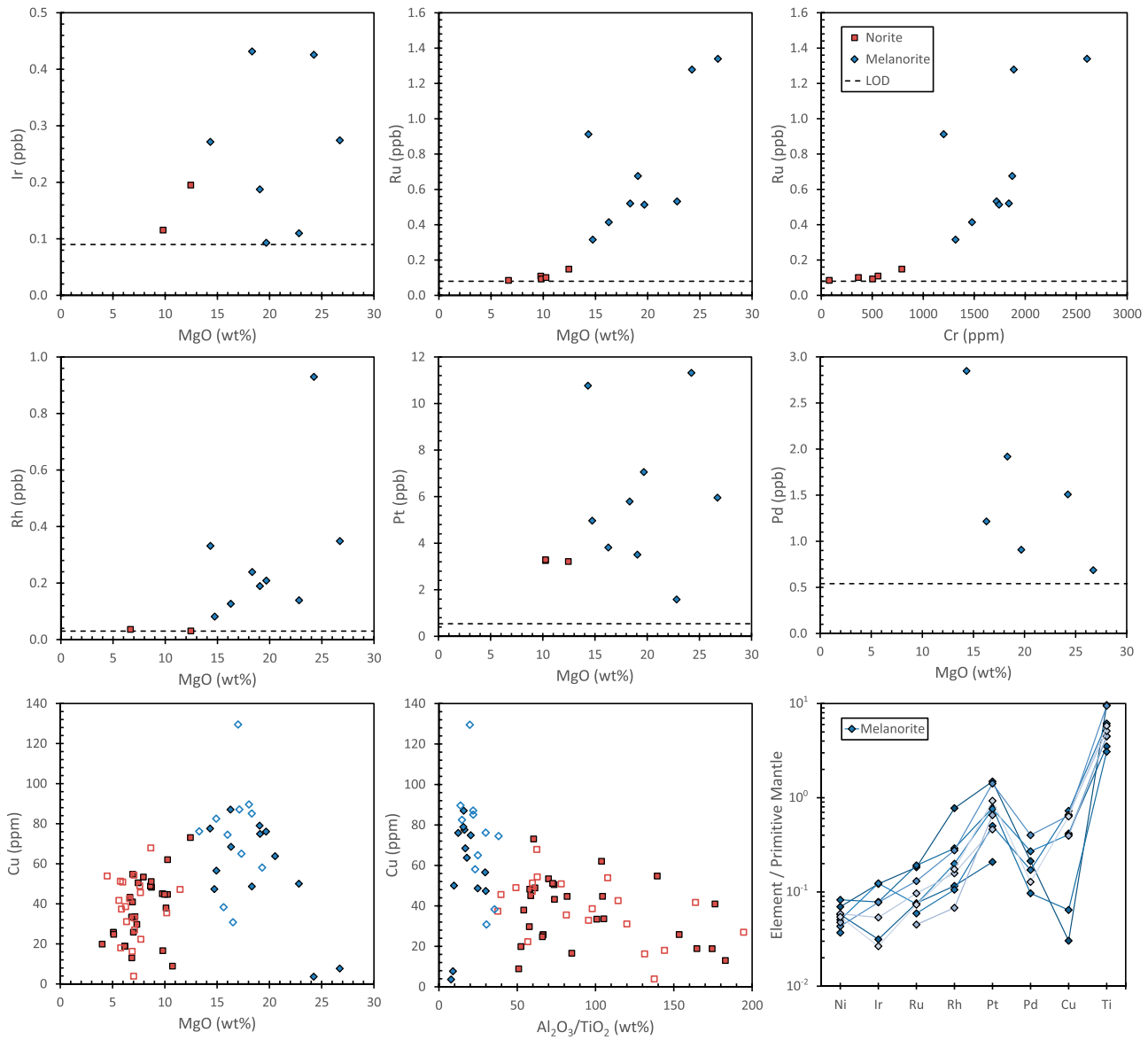

FIGURE 8 | Platinum group element (PGE) and Cu data for norite belt samples. Most norite sample PGE concentrations are below the limit of detection (LOD) and are not shown. LOD for PGEs shown as dashed lines. Solid and hollow symbols in Cu plots refer to WSU and ALS data, respectively. Multi-element patterns are only shown for melanorites, as most norite data were below LOD. Data are normalised to primitive mantle values of Becker et al. (2006) and Fischer-Gödde et al. (2011) for the PGEs, McDonough and Sun (1995) for other elements.

Both groups of samples have consistent, largely parallel REE and trace element patterns, with depleted HREE, highly enriched LREEs, and strong negative anomalies in Nb, Ta, and Ti. These patterns broadly parallel the average composition of felsic orthogneisses from the Maniitsoq region (Gardiner et al., 2019). Zirconium and Hf show variable anomalies in both groups, with Zr/Zr* ranging from 0.4–1.5 in the norites and from 0.5 to 10.3 in the melanorites ($Zr/Zr^* = 2 \times Zr_N/[Sm_N + Gd_N]$; Gd is used instead of Eu due to the presence of Eu anomalies). The norites show strong positive anomalies in Pb and Sr.

Platinum Group Element Data

Concentrations of PGEs (**Figure 8**; **Supplementary Table S1**) in the norites are low, with most samples close to or below the limit of detection (LOD) for most or all PGEs. The exception is Pt, with three samples showing values of ~3 ppb Pt. The melanorites have significantly higher PGE concentrations, with only Pd in three samples falling below the LOD. Iridium contents are low and broadly scattered. Ruthenium and Rh concentrations fall with decreasing MgO; Ru shows a strong correlation with Cr for some samples. Platinum and Pd are both scattered against MgO. Multi-

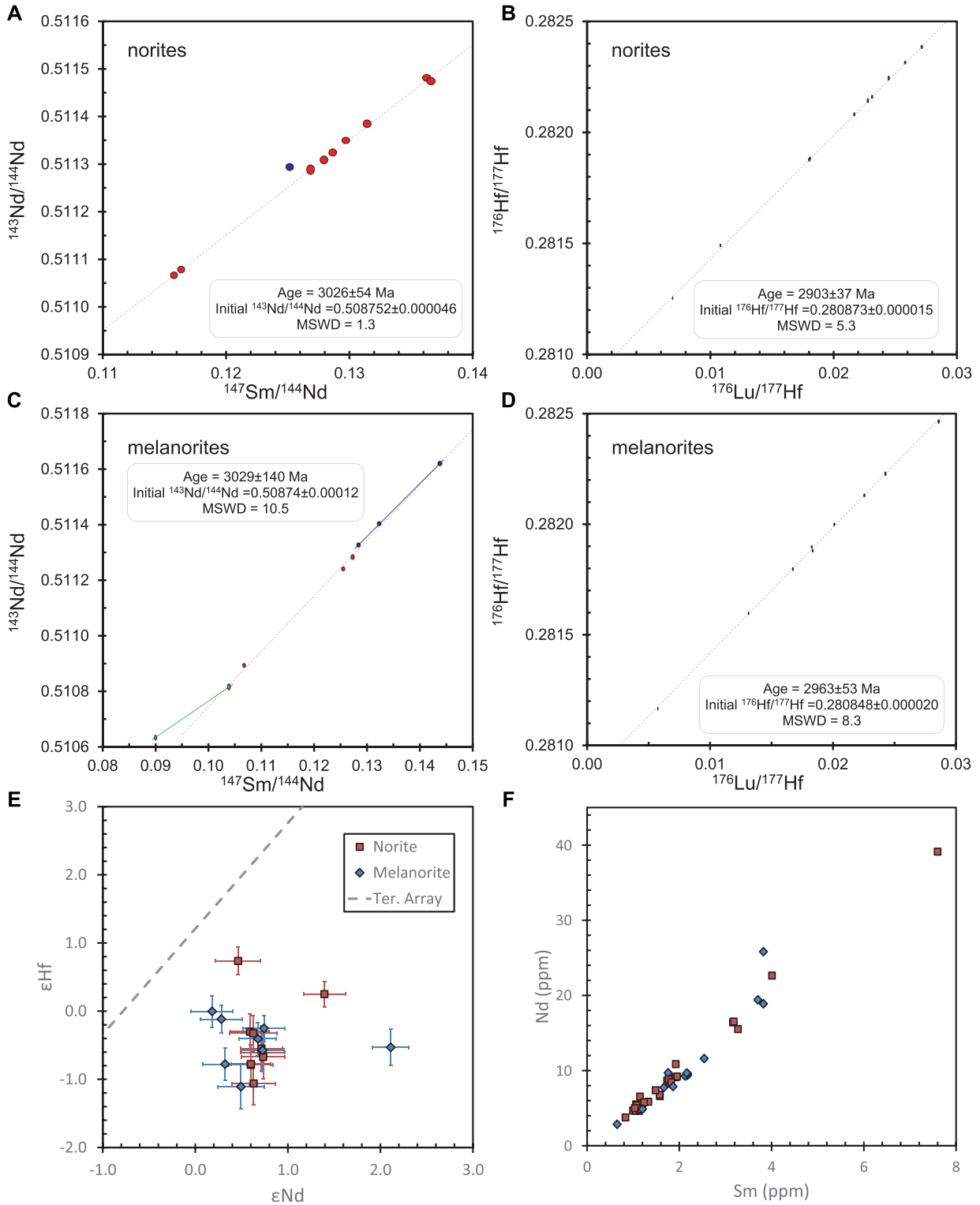

FIGURE 9 | (A) ^{147}Sm-^{143}Nd plot for norite samples. Most samples lie on an isochron, with the exception of sample 1,041 (blue symbol), which was excluded as it is an εNd outlier. **(B)** ^{176}Lu-^{176}Hf plot for norite samples, all samples form an errorchron. **(C)** ^{147}Sm-^{143}Nd plot for melanorite samples. Coloured lines and symbols of the same colour join samples from the same norite body. Red symbols are melanorites from bodies where only one sample was analysed. **(D)** ^{176}Lu-^{176}Hf plot for melanorite samples, all samples form an errorchron. All isochron plots generated using isoplot (Ludwig, 2012). **(E)** εNd and εHf data for norite and melanorite samples calculated at 3,010 ± 10 Ma with 2σ uncertainties propagated after Sambridge and Lambert (1997), excluding decay constant uncertainties. Terrestrial array of Vervoort et al. (2011) shown for reference. **(F)** Sm and Nd trace element concentration data for norites and melanorites.

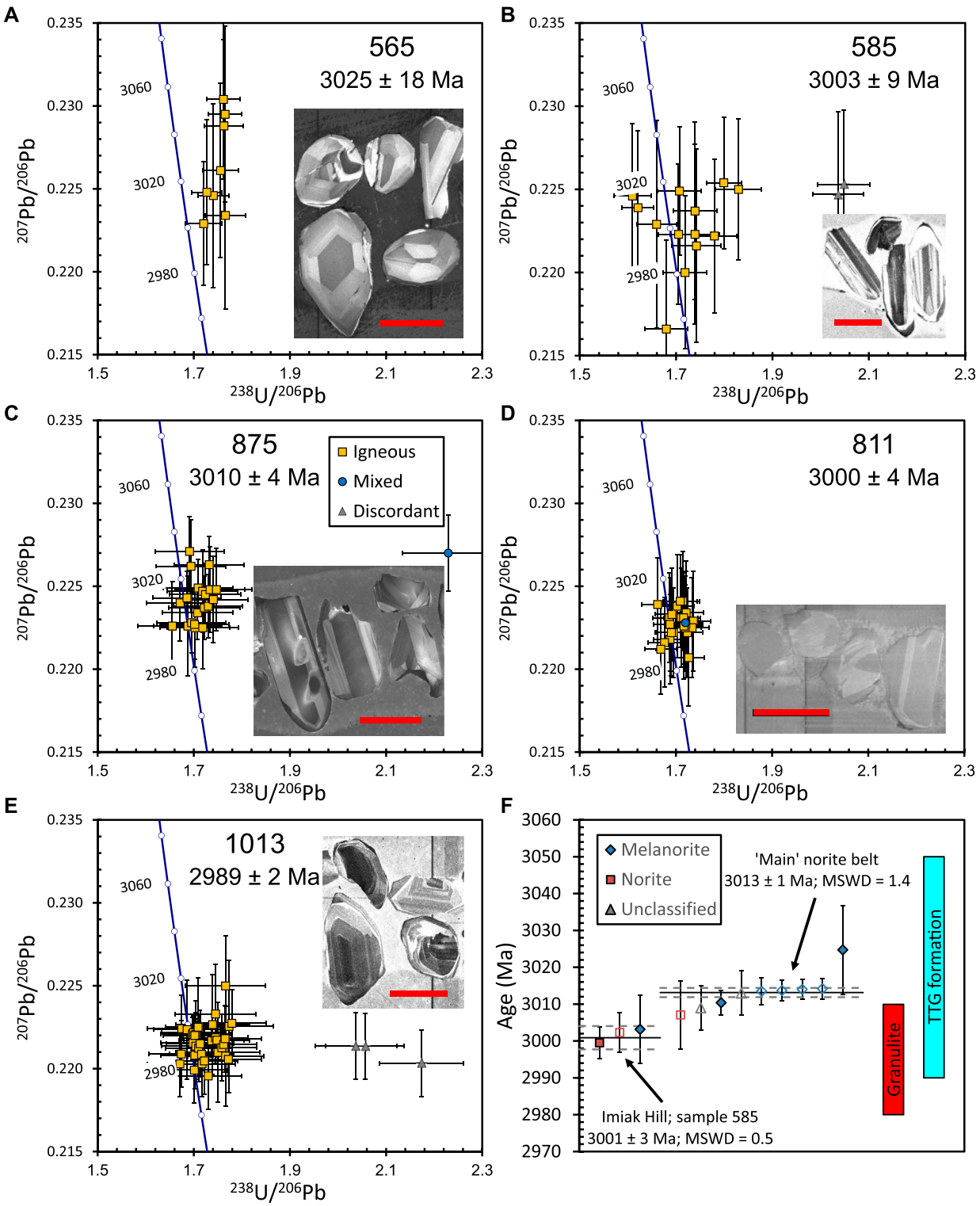

FIGURE 10 | Zircon U-Pb geochronology results. **(A)**–**(E)** Tera-Wasserburg concordia diagrams for dated samples, sample numbers given in upper right corner. Mixed and discordant analyses not included in calculations of mean $^{207}Pb/^{206}Pb$ ages. Insets show cathodoluminescence images of typical zircons from each sample, red scale bars = 100 μm. **(F)** Zircon U-Pb age summary showing all Maniitsoq Norite Belt ages from this study, Ravenelle et al. (2017), Gardiner et al. (2019), and Aarestrup et al. (in press) grouped according to sample type. Closed symbols are from this study, open symbols indicate previous work. Age range of granulite-facies metamorphism (Yakymchuk et al., 2020) and TTG formation (Gardiner et al., 2019) in the Akia Terrane is shown for comparison.

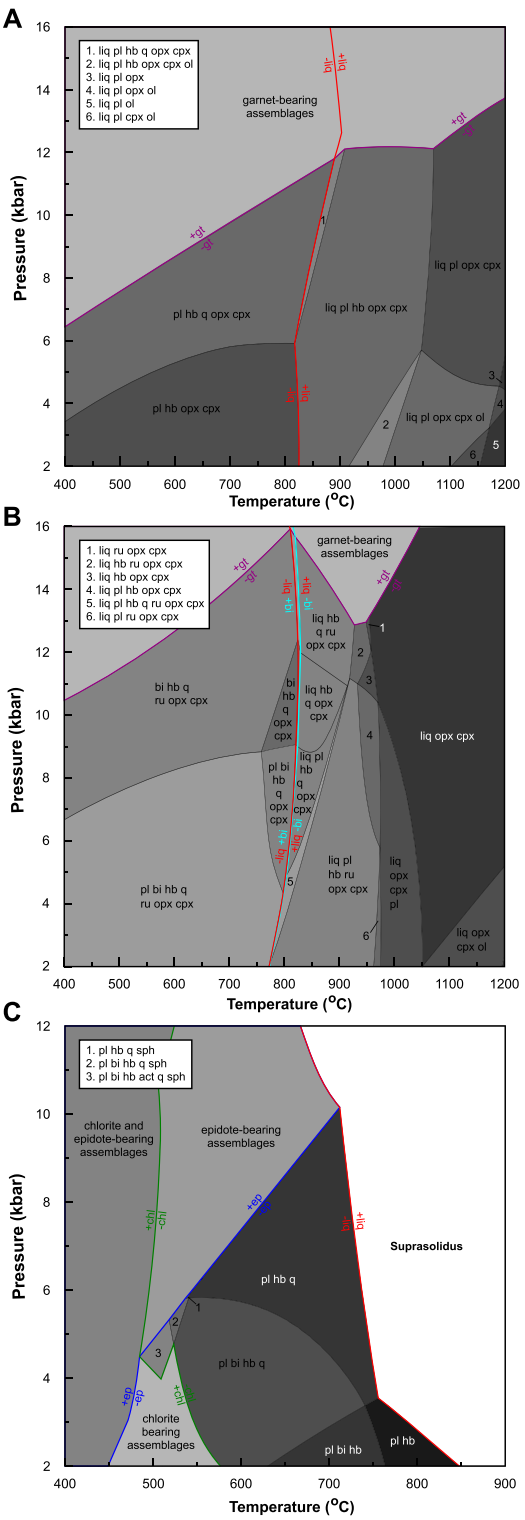

FIGURE 11 | Phase equilibria modelling and pyroxene thermobarometry constraints on metamorphic conditions of the norite belt. Opx = orthopyroxene, cpx = clinopyroxene, ol = olivine, pl = plagioclase, hb = hornblende, bi = biotite, q = quartz, ru = rutile, sph = sphene, liq = liquid. **(A)** Simplified P-T pseudosection for sample 1,045 (representative norite

(*Continued*)

element patterns for melanorite PGEs, Ni, Cu, and Ti, are scattered, with a general enrichment of Pt and Pd relative to Ir and Ru. Copper concentrations are also shown in **Figure 8**, and are generally higher in the melanorites than the norites, although the two most MgO-rich melanorite samples have very low Cu concentrations. Copper concentrations show a wide scatter in the norites when plotted against either MgO or Al_2O_3/TiO_2.

^{147}Sm-^{143}Nd and ^{176}Lu-^{176}Hf Isotopic Analyses

Initial $^{143}Nd/^{144}Nd$ and $^{176}Hf/^{177}Hf$ isotopic compositions were calculated using the decay constants of Lugmair and Marti (1978) for ^{147}Sm (uncertainty from Ickert, 2013 and Söderlund et al., 2004) for ^{176}Lu, to an age of 3,010 ± 10 Ma (*Age of the Maniitsoq Norite Belt*). εNd and εHf values were calculated relative to the chondritic uniform reservoir (CHUR) of Bouvier et al. (2008), with uncertainties propagated after Sambridge and Lambert (1997). The initial isotopic compositions of the two groups closely overlap. Most norites fall within a tight range between +0.5 and +0.7 εNd_{3010Ma}; one sample collected near an intrusive granite pegmatite has a higher εNd of +1.4 (2σ uncertainties are typically ~0.2 epsilon units, ~0.8 including decay constant uncertainty). Most melanorite εNd range from +0.2 to +0.7, one sample collected near an intrusive TTG sheet has a higher εNd of +2.1. Most norites show a range in εHf_{3010Ma} between −1.1 and −0.3; two samples collected adjacent to a granite pegmatite have higher εHf of +0.3 and +0.7. Melanorite εHf values are between −1.1 and 0.0 (typical 2σ uncertainties are ~0.3 epsilon units for Hf with or without decay constant uncertainties). All samples fall close to, but slightly below, the Hf-Nd terrestrial array (**Figure 9E**; Vervoort et al., 2011).

The ^{147}Sm-^{143}Nd data for the norites (excluding the sample with outlier εNd), define an isochron with an age of 3,026 ± 54 Ma (MSWD = 1.3; n = 9; **Figure 9A**). The initial Nd corresponds to εNd of 0.35 ± 0.90 at 3,010 Ma. Their ^{176}Lu-^{176}Hf data lie on an errorchron, with a younger apparent age of 2,903 ± 37 Ma (MSWD = 5.3; n = 10; **Figure 9B**).

With one outlier sample removed (sample 823, collected adjacent to an intrusive TTG sheet), the melanorites form an ^{147}Sm-^{143}Nd errorchron with apparent age of 3,029 ± 140 Ma (MSWD = 10.5; n = 8; **Figure 9C**). However, data from different melanorite bodies appear to lie on trends with shallower slopes. The melanorites also form an errorchron in ^{176}Lu-^{176}Hf space, with an apparent age of 2,963 ± 53 Ma (MSWD = 8.3; n = 9; **Figure 9D**).

FIGURE 11 | composition) assuming H_2O = loss on ignition. Garnet is not present in any norite sample, so garnet-bearing assemblages are not subdivided for simplicity. **(B)** Simplified P-T pseudosection for sample 1,427 (representative melanorite composition) assuming H_2O = loss on ignition. Garnet is not present in a melanorite sample; garnet-bearing assemblages are not subdivided. Biotite is lost at temperatures just above the liquidus; fields between liquid in and biotite out are not labelled. **(C)** Simplified P-T pseudosection under water saturated conditions for sample 1,045. Retrogressed samples do not contain chlorite or epidote; predicted assemblages containing these minerals are grouped for simplicity.

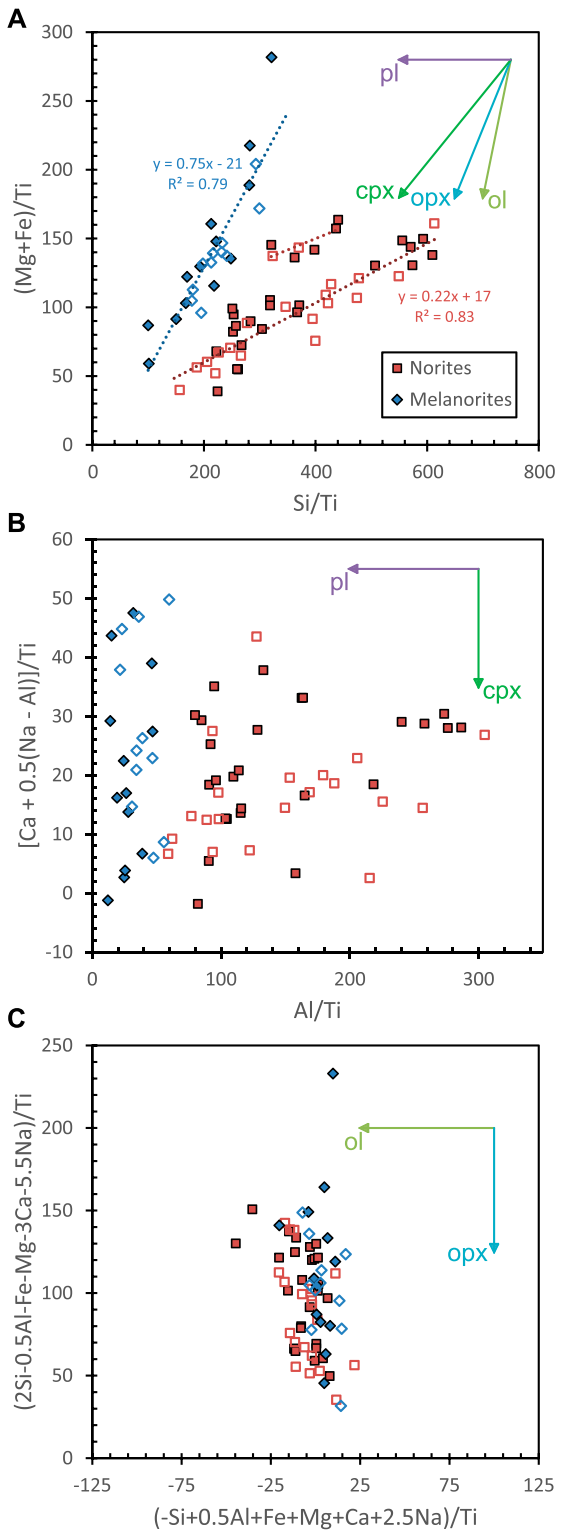

FIGURE 12 | Pearce element ratio plots for norite and melanorite samples (Pearce, 1968). Arrows show melt evolution due to loss of plagioclase (pl), clinopyroxene (cpx), orthopyroxene (opx), and olivine (ol). Titanium is used as a conservative element instead of K (Russell et al., 1990), due to likelihood of K mobility during metamorphism. **(A)** (Mg + Fe)/Ti

(*Continued*)

Oxygen Isotope Analyses

Bulk rock O isotopic compositions for Fossilik norites range from $\delta^{18}O$ of +5.9 to +7.0‰ (**Supplementary Table S1**; **Figure 13**), with typical 2σ uncertainties of <0.1‰. These values are slightly elevated relative to MORB (+5.4 to +5.8‰; Eiler et al., 2000). However, the highest $\delta^{18}O$ value is for a retrogressed sample (sample 1,048), and the range for samples with a predominantly granulite-facies mineral assemblage is more restricted, from $\delta^{18}O$ +5.9 to +6.6‰. Compositions of the two plagioclase separates analysed are 0.6 and 1.1‰ higher than their host samples, with $\delta^{18}O$ of +6.7 and +7.0‰, respectively.

U-Pb Zircon Geochronology

Zircon U-Pb analyses are presented for three norite belt samples dated by LA-ICP-MS, and one crosscutting TTG sheet dated by SHRIMP (**Figure 10**; **Supplementary Table S4**). Detailed zircon descriptions are given in the **Supplementary Material**. Sample 565, a melanorite from the southwest end of the belt, contains oscillatory-zoned zircon with minor later rim growth. Eight analyses of oscillatory-zoned zircon yielded a weighted mean $^{207}Pb/^{206}Pb$ age of 3,025 ± 12 Ma (MSWD = 1.5), interpreted as the magmatic crystallisation age. Sample 585, a mineralised melanorite recovered from drill core, contains oscillatory-zoned zircon with common high cathodoluminescence response rims. Thirteen analyses of oscillatory zoned zircon yielded a weighted mean $^{207}Pb/^{206}Pb$ age of 3,003 ± 9 Ma (MSWD = 1.0), interpreted as the magmatic crystallization age. Sample 875, a mineralised spotted norite from the northern part of the belt, contains sector- and oscillatory-zoned zircon; some grains contain small metamict xenocrystic cores. Twenty analyses of grains with well-developed sector and oscillatory zoning yielded a weighted mean $^{207}Pb/^{206}Pb$ age of 3,010 ± 3 Ma (MSWD = 1.5), interpreted as the magmatic crystallisation age. Sample 811, a coarse grained norite from Imiak Hill norite body (Ravenelle et al., 2017), located in the northern part of the norite belt, contains zircon with faint oscillatory and sector zoning. Twenty-two analyses of these zircons yielded a weighted mean $^{207}Pb/^{206}Pb$ age of 3,000 ± 4 Ma (MSWD = 0.40), interpreted as the magmatic crystallisation age. Sample 1,013 is from a TTG sheet intruding melanorites near the centre of the norite belt. Thirty-three analyses conducted on grains with oscillatory or sector zoning yield a weighed mean $^{207}Pb/^{206}Pb$ age of 2,989 ± 2 Ma (MSWD = 1.2), interpreted as the magmatic crystallisation age.

FIGURE 12 | against Si/Ti plot: plagioclase fractionation produces horizontal trends, clinopyroxene fractionation produces a trend with gradient = 0.5, orthopyroxene fractionation has a gradient = 1, olivine fractionation has a gradient = 2. **(B)** Plot for distinguishing plagioclase (horizontal trends) and clinopyroxene (vertical trends) fractionation. Olivine and orthopyroxene fractionation have no effect on this plot, as Al, Ca, and Na are conservative for fractionation of these minerals. **(C)** Plot for distinguishing orthopyroxene and olivine fractionation, both clinopyroxene and plagioclase fractionation produce vectors with zero length on this plot (Nicholls and Russell, 2016).

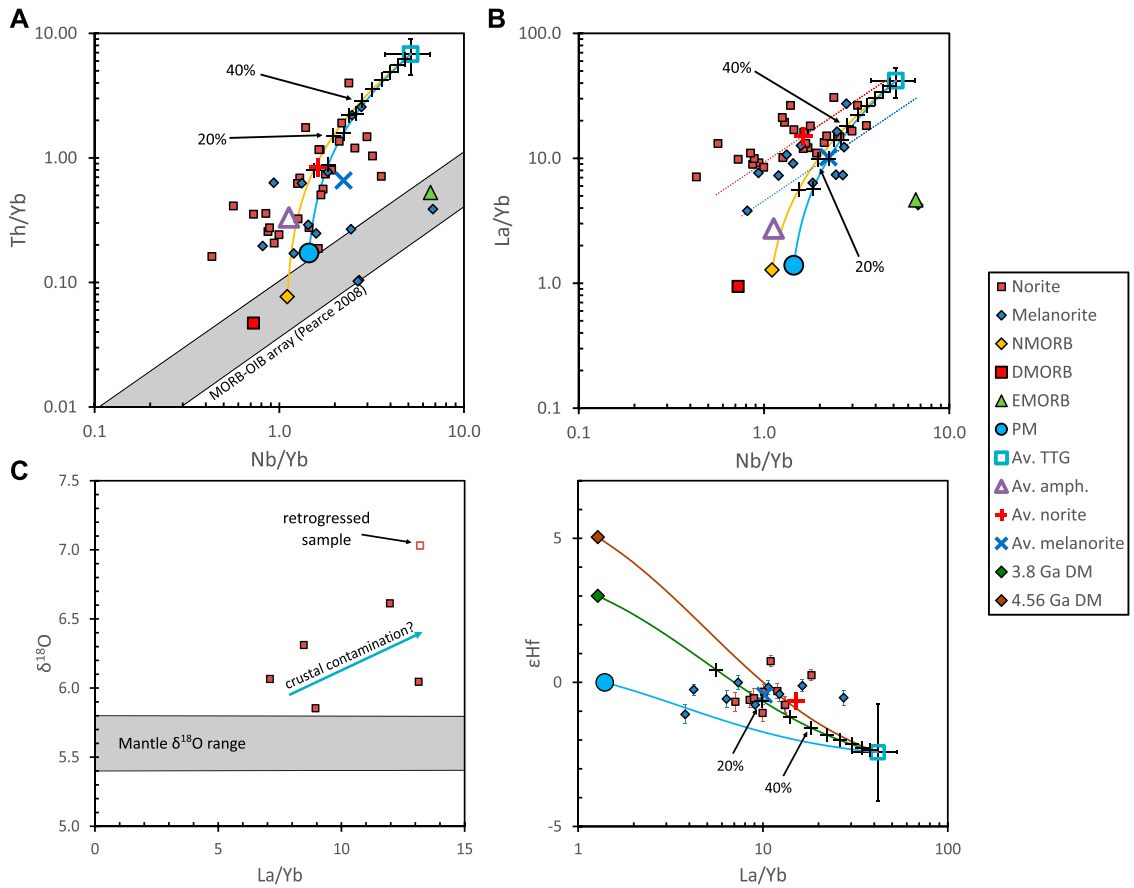

FIGURE 13 | Indicators and models of crustal contamination. **(A)** and **(B)** Trace element plots showing mixing between mantle-derived magmas and average felsic orthogneiss compositions in the Maniitsoq region ("Av. TTG"; Gardiner et al., 2019). Th/Yb and La/Yb are primarily sensitive to crustal contamination, whereas Nb/Yb gives an indication of source enrichment and degree of melting (Pearce, 2008). Primitive mantle (PM) composition is from Sun and McDonough (1989), MORB compositions are from Gale et al. (2013), concentrations are normalised to average Yb content in norite belt samples for mixture modelling. **(C)** $\delta^{18}O$ against La/Yb plot, $\delta^{18}O$ broadly increases with La/Yb, consistent with contamination by high $\delta^{18}O$ crustal rocks. Mantle range is from Eiler et al. (2000). **(D)** εHf plotted as a function of La/Yb. Average TTG εHf at 3.0 Ga is calculated from average value for zircons 2,900 Ma < age < 3,100 Ma from the Maniitsoq region (Gardiner et al., 2019). Primitive mantle isotopic composition is assumed to be identical to chondritic uniform reservoir (Bouvier et al., 2008) at 3.0 Ga "3.8 Ga DM" follows chondritic uniform reservoir (Bouvier et al., 2008) until 3.8 Ga, then evolves with depleted mantle $^{176}Lu/^{177}Hf$ of 0.03976 (Fisher and Vervoort, 2018; Spencer et al., 2020) to 3.0 Ga "4.56 Ga DM" evolves with depleted mantle $^{176}Lu/^{177}Hf$ 0.0384 (Griffin et al., 2000) from 4.56 until 3.0 Ga. Binary mixing models between hypothetical mantle derived magmas and average felsic orthogneisses are shown as curves, colour coded according to the modelled mantle source, black crosses indicate 10% increments in mixture.

Phase Equilibrium Modelling

The results of phase equilibrium modelling are presented in **Figure 11**. No garnet is present in any of the norite or melanorite samples, and no indications of anatexis were observed in any of the norite belt rocks. This limits the pressures of granulite metamorphism to <11 kbar for garnet- and melt-free assemblages modelled for norite sample 1,045 (**Figure 11A**). A poorly-constrained pressure of <16 kbar is obtained for garnet-free assemblages modelled for melanorite sample 1,427 (**Figure 11B**). The predicted solidus for sample 1,045 gives a maximum temperature of granulite metamorphism between ~825°C at pressures <6 kbar to ~875°C at 11 kbar. The predicted solidus for sample 1,427, and the presence of biotite in the melanorite granulite-facies assemblage, restricts the estimated peak temperatures to <825°C. However, the temperature of the modelled solidus is very sensitive to the concentration of H_2O in the bulk composition, which was determined from the LOI value. Considering that some H_2O may have been introduced during weathering or retrogression, the estimated solidus temperatures are probably minima and the granulite-facies temperatures may have been higher. However, the presence of biotite and hornblende in the granulite-facies assemblages suggests that these rocks were not completely anhydrous during metamorphism. Considering these caveats, the observed norite granulite-facies assemblage of plagioclase + orthopyroxene + clinopyroxene + hornblende + biotite ± quartz is restricted to a broad field with T < 875°C and 4 kbar < P <11 kbar. The observed melanorite granulite-facies assemblage of orthopyroxene + hornblende + plagioclase ± clinopyroxene ± biotite ± rutile is restricted to T < 800°C at P < 9 kbar.

A water saturated norite composition (sample 1,045) was also modelled to investigate the conditions of amphibolite-facies retrogression (**Figure 11C**). The retrogressed norite assemblage of plagioclase + hornblende + biotite ± quartz, with an absence of epidote and chlorite, restricts the metamorphic conditions to between ~525 and ~740°C, at relatively low pressures of <6 kbar.

DISCUSSION

Age of the Maniitsoq Norite Belt

Other Relevant Age Data

Direct Dating of Norite Belt Samples

Sample 173 was previously interpreted as part of the Finnefjeld Orthogneiss Complex (Gardiner et al., 2019). However, new mapping suggests that it is located outside the Finnefjeld Orthogneiss Complex, near the centre of the norite belt (**Figure 1**). A reinterpretation of field, petrographical, and geochemical evidence suggests it is a typical norite: friable, with moderate MgO contents (7.7 wt%), high SiO_2 contents (57 wt%) and a high Al_2O_3/TiO_2 ratio of 40. Gardiner et al. (2019) report a U-Pb zircon age of 3,007 ± 9 Ma, interpreted as the magmatic crystallisation age.

Geochronology samples from Ravenelle et al. (2017) are divided into our norite and melanorite groups on the basis of MgO and Cr contents (North American Nickel, unpublished data). Four U-Pb zircon dates are from samples with high MgO (>15 wt%) and Cr (>900 ppm) and are considered melanorites. These have ages of 3,014 ± 3 Ma (Fossilik), 3,014 ± 3 and 3,014 ± 3 Ma (two samples from Spotty Hill), and 3,014 ± 4 Ma (P-030—Nunanguit; Ravenelle et al., 2017). One date of 3,002 ± 5 Ma (Imiak Hill; Ravenelle et al., 2017) was obtained from a sample with relatively low MgO (7 wt%) and Cr contents (~160 ppm), which we interpret as a norite.

Aarestrup et al. (in press) present zircon U-Pb data for two additional norite belt samples, FOS2 and QUA, from the Fossilik and Imiak Hill complexes, respectively. It is not clear if these samples represent norites or melanorites. Both samples have bimodal $^{207}Pb/^{206}Pb$ age distributions, with oscillatory zoned zircon yielding older ages than recrystallised zircon. Oscillatory-zoned zircon analyses yield mean ages of 3,013 ± 6 Ma for FOS2 and 3,009 ± 6 Ma for QUA, interpreted as igneous crystallisation ages. Recrystallised domains yield mean ages of 2,995 ± 10 Ma for FOS2 and 2,999 ± 14 Ma for QUA, interpreted as metamorphic recrystallisation ages.

Ages of Host and Cross Cutting Tonalite-Trondhjemite-Granodiorites

Melanorite sample 565 (this study) is hosted in 3,018 ± 13 Ma tonalitic orthogneiss (sample 566; Gardiner et al., 2019), which provides a maximum age for the melanorites at this locality. It is also intruded by compositionally similar tonalite with an age of 2,998 ± 14 Ma (sample 567; Steenfelt et al., in review), providing a minimum age for these melanorites. Sample 582, is an orthogneiss that cross-cuts the Spotty Hill norite body. A zircon U-Pb age of 3,014 ± 8 Ma (Steenfelt et al., in review) provides a minimum age for the norites at this locality. Sample 1,256 is from a TTG sheet intruding norite represented by sample 1,257 (**Figure 2F**). A zircon U-Pb magmatic crystallization age of 3,003 ± 4 Ma (Kirkland et al., in review) provides a minimum age for the norites at this locality. Sample 1,260 is from an enclave of deformed TTG included within the same norite body (**Figure 2H**), whose layering is truncated by the norites. Its magmatic crystallisation age of 3,003 ± 4 Ma (Kirkland et al., in review) provides a maximum age for norites in this body.

Absolute Age of the Norite Belt

We combine U-Pb zircon ages for norite belt samples from this study with U-Pb zircon ages reported in Ravenelle et al. (2017), Gardiner et al. (2019), and Aarestrup et al. (in press) to establish an absolute age for the Maniitsoq Norite Belt. Taken together, U-Pb data exist for three norites, six melanorites, and two unclassified samples from the Maniitsoq Norite Belt. All of the dated samples contain dominant zircon populations with ages between 3,000 ± 4 and 3,025 ± 12 Ma; many ages overlap within uncertainty. However, a weighted mean of all samples (n = 12; metamorphic ages from Aarestrup et al., in press, are excluded) yields an age of 3,012 ± 3 Ma (2σ), but with a high MSWD of 5.7 ($p = 3 \times 10^{-9}$). This implies that the variation in ages across all dated samples is greater than expected based on analytical uncertainty alone. Weighted mean ages for only the norite samples dated in this study and analysed in the same lab by Gardiner et al. (2019) (3,007 ± 8 Ma; MSWD = 6.2; n = 5), and only the samples dated by Ravenelle et al. (2017) (3,013 ± 4 Ma; MSWD = 4.0; n = 5) also have high MSWD and low probabilities of fit ($p < 0.002$). As both datasets from different labs show a greater spread in ages than expected from analytical uncertainty, the excess spread in ages is unlikely to be due to systematic uncertainties or inter-lab biases, and we consider it unlikely that the dated samples come from the same age population.

Two dated samples from the Imiak Hill norite body (sample 811; Ravenelle et al., 2017) are the only samples that do not overlap within uncertainty with the weighted average age of all samples, with ages of 3,000 ± 4 and 3,002 ± 5 Ma. Sample 585 has a similar average age of 3,003 ± 9 Ma. Excluding these data, the remaining norite belt samples yield a weighted mean age of 3,013 ± 1 Ma (MSWD = 1.4; n = 9; $p = 0.19$), which we interpret as the magmatic emplacement age of the majority of the norite belt (**Figure 10F**).

The weighted mean age of the two Imiak Hill samples and sample 585 is 3,001 ± 3 Ma (MSWD = 0.5; n = 3; $p = 0.62$). We test whether this age is statistically resolvable from the rest of the belt using a Welch's *t*-test, which tests if two populations with different variances and sample sizes have the same mean. The *t* statistic for the weighted means is 13.1, corresponding to a probability of the mean ages being identical of 0.39%. The two ages are therefore distinguishable at the 95% confidence level, and we conclude that the samples from Imiak Hill and sample 585 are resolvably younger than the average age of the belt.

There are three possibilities for the observed age difference between the two groups of samples: 1) the apparently younger samples have the same emplacement age as the rest of the belt but zircon U-Pb ages were variably reset during metamorphism, either through metamorphic temperatures exceeding the Pb

blocking temperature of zircon, or by Pb loss from metamict zircon grains; 2) the apparently younger samples lacked igneous zircon, and the analysed zircons formed during granulite-facies metamorphism; 3) there were at least two magmatic pulses which formed the Maniitsoq Norite Belt, featuring intrusion of compositionally similar norites.

We rule out the possibility that U-Pb ages were reset by temperatures exceeding the Pb blocking temperature of zircon; if this was the case the all dated norite belt samples should be reset to the same age, particularly where sampling locations were closely spaced (**Figure 1**). Furthermore, calculated alpha doses (assuming that radiation damage would commence from the apparent crystallisation age) indicate that most grains have values consistent with crystalline zircon, suggesting there was no Pb loss due to metamictisation. We rule out a metamorphic origin for zircons in samples 585 and 811 on the basis that the grains contain sector and oscillatory zoning (**Figure 10**), and their Th/U ratios (1.6 ± 1.9 and 1.3 ± 0.5, respectively; 2σ uncertainty) are more consistent with igneous zircon growth than that of metamorphic zircons (Kirkland et al., 2015; Yakymchuk et al., 2018). Furthermore, these Th/U ratios are indistinguishable from zircon from the other norites and melanorites analysed in this study (Th/U from 1.3 ± 0.5 to 2.2 ± 2.2). Finally, cross cutting relationships and U-Pb ages for TTG samples 1,256 and 1,260 (see below) are consistent with an age of 3,003 ± 4 Ma for norites at a different locality, providing independent evidence for the existence of younger norites associated with the Maniitsoq Norite Belt. We conclude that there were at least two episodes of intrusion of compositionally similar norites, and that magmatism in the Maniitsoq Norite Belt was ongoing between at least ~3,013 and ~3,001 Ma. We note that some ages, in particular samples 173 (3,007 ± 9 Ma; Gardiner et al., 2019) and QUA (3,009 ± 6 Ma; Aarestrup et al., in press) appear to fall between the two age groups and overlap both of the average ages within 2σ uncertainties. However, at this level of age resolution, we cannot distinguish whether these represent further episodes of norite intrusion, or whether they belong to the ~3,013 or ~3,001 Ma magmatic pulses.

Relative Age of the Norite Belt and Tonalite-Trondhjemite-Granodiorites

Field observations indicate that the norites post-date and intruded deformed TTG gneisses, but were in turn intruded by later TTG melts before the end of regional deformation (*Field Observations and Sampling*). The range of ages for TTGs in the Maniitsoq region are consistent with these observations. TTG formation is recorded between ~3,050 and 2,990 Ma (Garde, 1997; Garde et al., 2000; Gardiner et al., 2019), occurring both before and after the formation of the norite belt. Locally, field relationships of dated samples also support this chronology. Melanorite sample 565 is hosted in tonalitic gneiss (3,018 ± 13; sample 566; Gardiner et al., 2019) with an overlapping, but slightly older, age than the norite belt average (3,013 ± 1 Ma), and is in turn intruded by tonalite with a slightly younger age of 2,998 ± 14 Ma (sample 567; Steenfelt et al., in review). Similarly, norite represented by sample 1,257 contains enclaves of deformed TTG orthogneiss with a magmatic age of 3,003 ± 4 Ma (sample 1,260; Kirkland et al., in review), and is in turn intruded by a TTG sheet with an indistinguishable age of 3,003 ± 4 Ma (sample 1,256; Kirkland et al., in review). The 3,014 ± 3 Ma melanorites in the Spotty Hill body (Ravenelle et al., 2017) are intruded by orthogneiss with an indistinguishable age of 3,014 ± 8 Ma (Steenfelt et al., in review). Finally, the youngest dated TTG intruding norite has an age of 2,989 ± 2 Ma (sample 1,013). These relationships indicate that the norites and melanorites were intruded into existing deformed TTG crust during ongoing TTG production and deformation, and that the formation of norite and one phase of TTG was essentially synchronous (within age resolution of the available zircon U-Pb data).

Metamorphism and Alteration of the Maniitsoq Norite Belt

Though previous studies have interpreted textures and mineral assemblages in the Maniitsoq Norite Belt as representing primary igneous features (Garde et al., 2012, Garde et al., 2013), several independent lines of evidence demonstrate that the norites and melanorites were strongly affected by later metamorphism. There is a preponderance of granoblastic textures, with no evidence of preserved solid-melt dihedral angles, igneous mineral zoning or previously reported skeletal/proto-orbicular textures (*Petrography*). Mineral assemblages are consistent with granulite-facies or retrogressed amphibolite-facies conditions, and pyroxene compositions show equilibration at granulite-facies conditions (*Phase Equilibrium Modelling* and *Peak Metamorphic Conditions*). Finally, despite geochemical evidence for chromite fractionation (*Magmatic processes in the Maniitsoq Norite Belt*), chromite is not found in norite belt samples, with only rare Cr-rich magnetite grains remaining (*Petrography*). We therefore attempt to constrain the peak metamorphic conditions and the effect of this metamorphism on norite belt geochemistry below.

Peak Metamorphic Conditions

Combining the phase equilibrium modelling results for norite sample 1,045 and melanorite sample 1,427, the granulite-facies metamorphic conditions are restricted to temperatures of <800°C and pressures <9 kbar (**Figure 11**). However, as noted previously, these maximum temperatures are loosely constrained, due to the strong effect of H_2O on the solidus, potentially introduced after peak metamorphism. Two-pyroxene thermobarometry (Lindsley and Andersen, 1983) provides an independent constraint on peak metamorphic temperatures, suggesting that pyroxenes equilibrated at temperatures of ~780 ± 70°C in the norites, and ~830 ± 70°C in the melanorites (**Supplementary Material**). These conditions are broadly consistent with those reported by Yakymchuk et al. (2020), who constrained the conditions of granulite-facies metamorphism to temperatures >800°C at pressures <9 kbar based on phase equilibrium modelling of metabasites. Given the uncertainty in the maximum temperatures in this study, the variation of minimum temperatures reported by Yakymchuk et al. (2020), and the possibility that temperatures varied spatially, it is difficult to assign a precise peak temperature for metamorphism in the

Maniitsoq Norite Belt. However, the coincidence of maximum temperatures from this study and minimum temperatures from Yakymchuk et al. (2020) suggest a peak temperature of ~800°C.

These peak metamorphic conditions were reached between ~3,010 and ~2,980 Ma (Yakymchuk et al., 2020), consistent with metamorphic zircon ages of 2,995 ± 10 and 2,999 ± 14 Ma in the norite belt (Aarestrup et al., in press). The timing of peak metamorphic conditions closely following norite belt formation suggests that the norite magmas were emplaced into very hot crust, and these high ambient temperatures permitted prolonged metamorphism. The low pressures (<9 kbar) established for this metamorphism require extremely high thermal gradients in the Akia terrane crust (>900°C/GPa for a peak temperature of 800°C), which suggests the Akia Terrane crust and lithosphere was thin at ~3.0 Ga (Sandiford and Powell, 1991; Yakymchuk et al., 2020). This inference is consistent with studies of mantle xenoliths from kimberlites in the Maniitsoq region, which show no evidence of lithospheric mantle older than 2.5 Ga (Wittig et al., 2010). Taken together, this suggests that the present day thick lithosphere beneath the Maniitsoq region formed after the end of major crust forming events in the Akia Terrane at ~3.0 Ga (Gardiner et al., 2019).

Effect of Metamorphism on Trace Elements

We assess the effect of metamorphism on the incompatible trace element compositions of the norites and melanorites by plotting all the analysed trace elements against an immobile element. As HFSEs typically used to assess element mobility (such as Zr) have scattered relationships with MgO and Al_2O_3/TiO_2 (**Figures 5, 6**), the trace elements are plotted against Yb (**Supplementary Material**). Rare-earth elements heavier than Dy show very strong correlations with Yb; the strength of these correlations decreases towards the LREEs. Europium shows more scatter than Sm or Gd and variable positive and negative Eu anomalies (**Figure 7**). This may suggest that the LREEs and MREEs were mobile to varying degrees during metamorphism, though this is complicated by evidence of plagioclase accumulation in the norites (*Magmatic Processes in the Maniitsoq Norite Belt*) and the likelihood that the samples experienced crustal contamination (*Crustal Contamination*).

Some other trace elements, such as Y and the HFSEs Nb, Zr, Hf, and Ti, show broad positive correlations with Yb (with some outliers; **Supplementary Material**). This is likely complicated by fractionation of minerals such as zircon (*Magmatic Processes in the Maniitsoq Norite Belt*), but we interpret these elements as largely immobile during metamorphism. Others such as the LILEs, Ta, Th, and U, show high degrees of scatter against Yb. While the LILEs were likely remobilised during metamorphism, assessment of Ta, T, and U mobility is difficult due to the effects of crustal contamination (*Crustal Contamination*).

Effect of Metamorphism on O Isotopes

The highest $\delta^{18}O$ value was observed for a retrogressed sample, which suggests that it was affected by low-temperature interaction with crustal fluids during retrogression. The remaining samples have $\delta^{18}O$ ranging from +5.9 to +6.6‰, slightly above values expected for mantle-derived magmas (Eiler et al., 2000), which could suggest that O isotopes in these samples were also modified during metamorphism. However, the elevated $\delta^{18}O$ values measured in these samples might be also inherited from assimilation of high-$\delta^{18}O$ crustal rocks such as TTGs (Whalen et al., 2002; Hiess et al., 2009; Vezinet et al., 2018). The O isotope fractionation between plagioclase and bulk rock of +0.6 to +1.1‰ indicates preservation of high-temperature equilibrium (Zhao and Zheng, 2003). Given previous observations that oxygen isotope compositions can be preserved through high grade metamorphism (Barnicoat and Cartwright, 1997), we interpret the elevated $\delta^{18}O$ relative to mantle values as resulting from crustal contamination (*Crustal Contamination*; **Figure 13**).

Interpretation of ^{147}Sm-^{143}Nd and ^{176}Lu-^{176}Hf Isotopes

Most of the ^{147}Sm-^{143}Nd and ^{176}Lu-^{176}Hf isotopic data does not form isochronous relationships (**Figure 9**), indicating that either these isotopic systems were disturbed during metamorphism, or that the isochron assumption of a constant initial isotopic composition was not met. In the melanorites, the ^{147}Sm-^{143}Nd system was likely disturbed on the scale of individual samples, as evidenced by the data arrays from each body having lower gradients (younger ages) than the errorchron comprising all of the data. The errorchron through most samples (excluding 823; 3,029 ± 140 Ma), lies within uncertainty of both the zircon age of the melanorites and the timing of peak metamorphism. This indicates that the ^{147}Sm-^{143}Nd system was either more or less closed at the scale of the melanorite bodies, or was reset on a large scale during peak metamorphism at ~3,010–2,980 Ma. The ^{176}Lu-^{176}Hf errorchron age of 2,963 ± 53 Ma is slightly younger than, but overlaps within uncertainty, both the timing of peak metamorphism and the zircon age of the norite belt. Given the abundance of zircons retaining magmatic ages older than the age of peak metamorphism, and the important role of zircon in controlling bulk rock Hf budgets (e.g., Belousova et al., 2002), it is unlikely that there was widespread open-system behaviour of Lu-Hf during peak metamorphism. We therefore interpret this errorchron age as a spurious age due to failure of the isochron assumption of constant initial $^{176}Hf/^{177}Hf$, either arising from variable crustal contamination of the melanorites (*Crustal Contamination*), potentially accompanied by zircon fractionation (*Magmatic Processes in the Maniitsoq Norite Belt*), or variations in the $^{176}Hf/^{177}Hf$ of the melanorite parental magmas.

We interpret the behaviour of the ^{147}Sm-^{143}Nd and ^{176}Lu-^{176}Hf systems in norite samples from the Fossilik body in a similar manner. The ^{147}Sm-^{143}Nd data forms an isochron (3.026 ± 54 Ma) within uncertainty of both the magmatic age of the norites and the timing of peak metamorphism, whereas the ^{176}Lu-^{176}Hf data form an errorchron. The ^{147}Sm-^{143}Nd isochron either represents closed system behaviour of the Sm-Nd system since the magmatic emplacement of the Fossilik body, or complete homogenisation of the $^{143}Nd/^{144}Nd$ ratio across the Fossilik intrusion during peak metamorphism (Hammerli et al., 2019). The overlapping timing of these two events makes them indistinguishable from these data. The Lu-Hf errorchron apparent age of 2,903 ± 37 Ma does not overlap with any known magmatic or igneous event in the Akia Terrane (*The Akia Terrane*), and so we interpret it as a spurious age arising

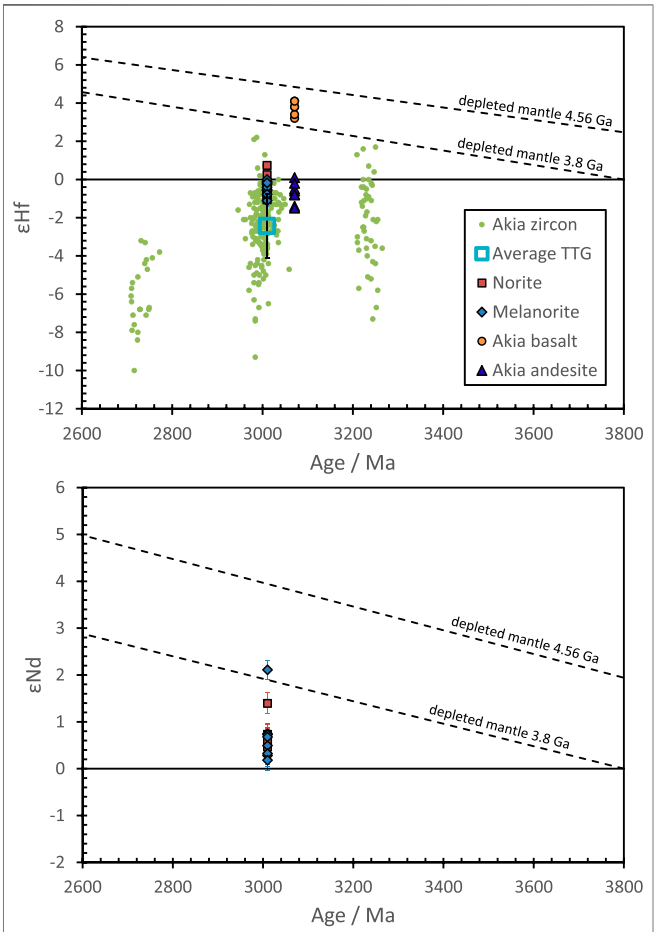

FIGURE 14 | Nd and Hf evolution curves for the Maniitsoq Norite Belt. εNd and εHf values for norite and melanorite data are calculated at 3,010 ± 10 Ma with 2σ uncertainties propagated after Sambridge and Lambert (1997). Zircon εHf data from the Maniitsoq region and average value for zircons 2,900 Ma < age < 3,100 Ma (Gardiner et al., 2019) are shown for comparison, uncertainty on average is 2σ. εHf data for basalts and andesites from the Akia Terrane are also shown for comparison (Szilas et al., 2017). Depleted mantle models for εHf are described in **Figure 13** and the main text. Approximate depleted mantle models for εNd are shown for reference. These follow chondritic uniform reservoir (Bouvier et al., 2008) until 3.8 and 4.56 Ga, respectively, before evolving with depleted mantle $^{147}Sm/^{143}Nd$ of 0.2156 (Vervoort and Blichert-Toft, 1999).

from variable crustal contamination possibly accompanied by zircon fractionation, or variations in the $^{176}Hf/^{177}Hf$ of the norite parental magmas.

Despite the possibility that $^{143}Nd/^{144}Nd$ ratios were homogenised or partially reset during granulite-facies metamorphism, the small difference in age between the emplacement of the Maniitsoq Norite Belt and the timing of peak metamorphism means that calculated εNd should be representative of the isotopic compositions before metamorphism, providing the Sm/Nd ratios were not strongly fractionated during metamorphism. Concentrations of Sm and Nd are strongly correlated for all samples (**Figure 9F**), so we consider it unlikely that this occurred, and believe the εNd to be broadly representative of the igneous protoliths of the norite belt.

Magmatic Processes in the Maniitsoq Norite Belt

The observed mineral assemblages in the Maniitsoq Norite Belt reflect metamorphism at granulite-facies or amphibolite-facies retrogression. However, to understand the petrogenesis of these samples, it is important to establish what mineral phases were fractionating in the igneous protoliths of these rocks. We attempt to constrain this below by considering the relationships between different elements and elemental ratios in the norites and melanorites.

Plagioclase Fractionation

The norites show trends towards plagioclase compositions in plots against MgO, trends towards highly suprachondritic Al_2O_3/TiO_2, and correlations between Al_2O_3/TiO_2 and Sr and Eu/Eu*, suggesting that plagioclase accumulation was an important control on norite bulk rock compositions (**Figures 4, 6**). Conversely, all melanorite samples have negative Eu anomalies. The largest of these anomalies (Eu/Eu* = 0.5) is found in a retrogressed sample, and likely reflects the higher mobility of Eu relative to other REEs during metamorphism (Bau, 1991). However, all other samples show a weak (R^2 = 0.35), but statistically significant correlation with MgO (critical R^2 value for 12 samples, 95% confidence = 0.33). This suggests that all melanorites experienced plagioclase fractionation, with the highest MgO samples undergoing the greatest plagioclase loss.

We correct for this plagioclase fractionation by regressing the Eu/Eu* data against Al_2O_3/TiO_2 back to an assumed parental melt composition with Eu/Eu* = 1 (i.e., no Eu anomaly). For the norites, this regression yields a parental melt (before plagioclase accumulation) with mean Al_2O_3/TiO_2 = 57 (36 < Al_2O_3/TiO_2 < 70, calculated from regression 95% confidence limits). For the melanorites, this regression yields a parental melt with mean Al_2O_3/TiO_2 = 45 (33 < Al_2O_3/TiO_2 < 120). This closely overlaps the Al_2O_3/TiO_2 ratios calculated for the norites, and is consistent with the norites and melanorites forming from the same parental melt, as inferred from field relationships (*Field Observations and Sampling*).

Nineteen of the 45 analysed norite samples lie in the range of 36 < Al_2O_3/TiO_2 < 70 (i.e., no detectable plagioclase accumulation), though five of these lie on the trend of increasing trace element concentrations at constant Al_2O_3/TiO_2 and are also excluded. The remaining 14 samples were averaged to approximate the composition of the parental melt before plagioclase accumulation. The norite bulk rock compositions for HREEs (**Figure 6**) lie on mixing lines between this melt composition and the average plagioclase composition analysed by EPMA. The extreme Al_2O_3/TiO_2 ratios observed in some norites indicate up to almost 60 wt% cumulus plagioclase (by weight) in some samples, which causes a "dilution" effect of trace element concentrations in the bulk rock due to a decreasing volume of intercumulus melt. LREEs such as La (**Figure 6**) are more scattered and show a flat to slightly increasing trend against Al_2O_3/TiO_2 in samples with a high degree of plagioclase accumulation. This may represent greater mobility of La during metamorphism or that the plagioclase accumulation was accompanied by crustal contamination (*Crustal Contamination*).

The second of the diverging trace element trends in the norites, towards increasing trace element concentrations at approximately constant Al_2O_3/TiO_2 (**Figure 6**) cannot be explained by plagioclase accumulation. Instead, based on the uniform enrichment in most trace elements (**Figure 7**), we interpret this to represent either incorporation of more evolved magma or a higher ratio of melt:phenocrysts in the igneous protoliths of these samples. The sample with the highest overall REE contents (sample 889) also has the largest negative Eu anomaly ($Eu/Eu^* = 0.5$), suggesting it incorporated an evolved melt that had undergone significant plagioclase fractionation.

Pyroxene Fractionation

In contrast to the norites, melanorite compositions are largely controlled by pyroxene fractionation. Major element variations form scattered trends towards orthopyroxene compositions, and the highest MgO samples (~23–27 wt% MgO) have compositions close to orthopyroxene compositions measured by EPMA (**Figure 4**). One of these samples shows a "cumulate-like" REE pattern with MREE < HREE (**Figure 7**), suggesting it incorporated little interstitial melt. Scandium and CaO, compatible in clinopyroxene (e.g., Bédard, 2001) are correlated in the melanorites (**Figure 6**), and on a Pearce element ratio plot of molar (Mg + Fe)/Ti against Si/Ti the melanorites fall on an array with a gradient of 0.75, between that expected for clinopyroxene or orthopyroxene fractionation alone (diopside gradient = 0.5, orthopyroxene gradient = 1; **Figure 12A**; Pearce, 1968; Russell et al., 1990). Large vertical variations in a plot of [Ca + 0.5(Na − Al)]/Ti against Al/Ti), designed to discriminate plagioclase from clinopyroxene fractionation (**Figure 12B**; Russell et al., 1990), and in an olivine-orthopyroxene discrimination plot (**Figure 12C**; Nicholls and Russell, 2016), confirm the importance of both clino- and orthopyroxene fractionation in generating the range of melanorite compositions. There is no evidence of olivine fractionation, which would be expected to drive increases in SiO_2 with falling MgO content (**Figure 4**).

In the norites, Sc is strongly scattered about plagioclase accumulation trends, and the positive gradient of 0.22 on a Pearce element ratio plot of molar (Mg + Fe)/Ti against Si/Ti (**Figure 12A**) cannot be explained by plagioclase accumulation alone (gradient = 0). This suggests that pyroxene was also a fractionating phase during the formation of the norites. A slight trend towards decreasing CaO with decreasing MgO (**Figure 4**), and scatter in a plot of [Ca + 0.5(Na − Al)]/Ti against Al/Ti (**Figure 12B**), confirms that clinopyroxene was a fractionating phase. Vertical variations on the olivine-orthopyroxene discrimination plot (**Figure 12C**), indicate that orthopyroxene was also fractionated during differentiation of the norites. Higher concentrations of Sc and MgO in the melanorites relative to the norites are consistent with overall pyroxene loss from the norites and accumulation in the melanorites.

Accumulation of Dense Accessory Phases in the Melanorites

HFSEs such as Zr, Hf, and Nb, which are usually expected to be immobile during metamorphism, are also highly scattered about plagioclase and pyroxene accumulation trends (**Figures 5, 6**). The norites and melanorites both show variable Zr anomalies with Zr/Zr^* of 0.4–1.5 (mean = 0.7) and 0.5–10.3 (mean = 1.6), respectively. The melanorites have higher mean Zr contents (52 ppm) than the norites (mean Zr = 29 ppm). However, considering only samples with no Zr anomaly ($0.9 < Zr/Zr^* < 1.1$), the norites and melanorites have indistinguishable mean Zr concentrations of 42 and 45 ppm, respectively, again consistent with both groups forming from the same parental melt. In conjunction with a strong correlation between Zr and Hf (**Figure 6**), we interpret this to suggest that zircon was a fractionating phase in the norites and melanorites, with the melanorites experiencing net accumulation of zircon, and the norites experiencing net zircon loss. The correlation between Cr an Ru in the melanorites (**Figure 8**) suggest that chromite was also a fractionating phase (e.g., Pagé and Barnes, 2016). Lower concentrations of Ru and Cr in the norites suggest that chromite was lost from the norites and accumulated in the melanorites.

Similar inferences can be made for sulphides in the Maniitsoq Norite Belt. Norites analysed in this study have low concentrations of both iridium-PGEs (IPGEs) and platinum-PGEs (PPGEs) relative to the melanorites (**Figure 8**). As PPGEs are thought to behave incompatibly in the absence of sulphide (Barnes et al., 1985), this cannot be explained solely by fractionation of early IPGE-bearing phases (e.g., chromite, laurite). Instead, we interpret this to reflect saturation of the norite parental magma in sulphide, which predominantly accumulated in the melanorites. This is consistent with generally lower Cu contents in the norites, scattered trends in Cu against Al_2O_3/TiO_2 and MgO, and the observation that mineralisation in the norite belt is predominantly concentrated in the high MgO melanorites (Ravenelle et al., 2017).

Relationship Between the Norites and Melanorites

The norites and melanorites appear to have had an extremely similar fractionating assemblage dominated by plagioclase, orthopyroxene and clinopyroxene. All major and trace element data are consistent with the norites and melanorites deriving from the same parental melt, and the two groups have closely overlapping εNd and εHf values. The main difference between the two is that the norites largely experienced plagioclase accumulation, and loss of dense phases such as pyroxene, zircon, chromite, and sulphide. These dense phases accumulated in the melanorites, which experienced plagioclase loss. We therefore interpret the norites and melanorites as complementary suites derived from the same parental melts, driven to different compositions by density driven segregation and accumulation of different minerals. This is interpretation is consistent with the observation that norites are found towards the palaeo-top of the Fossilik intrusion, whereas melanorites are found towards the base (Ravenelle et al., 2017).

Crustal Contamination

Enclaves of amphibolite and TTGs included in the norite belt, hybridised contact zones between norites and TTGs (**Figure 2**), and the presence of xenocrystic zircon cores, suggest that the

igneous protoliths of the norite belt experienced crustal contamination during their emplacement. Several geochemical and isotopic features of the norites and melanorites support this view. The norite belt samples are silicic (average of all samples = 54 wt% SiO_2) despite having ultramafic characteristics such as high Mg#, high Cr and Ni contents, and low concentrations of HREEs and HFSEs (Garde, 1997; Garde et al., 2012, Garde et al., 2013). Trace element proxies for crustal contamination of norite belt samples, such as Th/Yb and La/Yb (**Figures 13A,B**; Pearce, 2008), form broad arrays between depleted mantle melts (e.g., normal MORB (N-MORB)-like compositions) and the average composition of felsic orthogneisses in the Maniitsoq region (Gardiner et al., 2019), though there is significant scatter due to variable amounts of crystal fractionation accompanying this contamination. Similarly, the trace element patterns of the norites and melanorites closely resemble those of the average Maniitsoq felsic orthogneiss composition (**Figure 7**). Furthermore, the analysed norite samples have elevated $\delta^{18}O$ values relative to mantle values (**Figure 13C**), which broadly correlate with trace element indicators of crustal contamination, consistent with input of crustal materials. Finally, εNd and εHf values are low relatively to depleted mantle at 3 Ga, and εHf data form arrays between depleted mantle and Maniitsoq TTGs at 3 Ga (**Figure 14**).

The trace element compositions of the norites and melanorites allows us to place constraints on the nature of this crustal contaminant. The average composition of amphibolites analysed in the Maniitsoq region is far too low in incompatible trace elements such as La and Th to produce the array of norite and melanorite compositions (**Figure 13**). While this does not definitively rule out a contribution from mafic crustal contaminants, it does require the involvement of more evolved rocks, such as the regional TTG gneisses.

The Nb/Yb ratios of norite belt samples are inconsistent with melts derived from an enriched mantle source, or low degree melts enriched in incompatible elements (**Figures 13A,B**). We therefore calculate the approximate extent of crustal contamination that the norite belt protoliths underwent, assuming the parental melt was derived from a depleted mantle source (NMORB of Gale et al., 2013), or a high degree melt of a primitive mantle source ("flat" trace element pattern with trace element ratios equal to primitive mantle; Sun and McDonough, 1989). Both parental melt compositions are normalised to the average Yb concentration of the norites and melanorites, and contamination is modelled by binary mixing with the average local felsic orthogneiss composition. As there is considerable scatter due to the effects of fractional crystallisation, mineral accumulation, and metamorphism, we stress that these calculations are necessarily approximate, and rely on average norite and melanorite compositions rather than data for individual samples. Th/Yb relationships (**Figure 13A**) indicate the average norite and melanorite compositions require approximately 10% crustal contamination of either a depleted mantle- or primitive mantle-derived melt, though data are highly scattered, potentially due to the effects of zircon fractionation and/or Th mobility during metamorphism. La/Yb relationships are less scattered, although arrays of data along lines with gradients ≈1 in the La/Yb against Nb/Yb plot (**Figure 13B**) suggest fractionation of Yb relative to La and Nb during crystallisation of the norites and melanorites, possibly due to pyroxene fractionation. These data indicate ~20–30% crustal contamination was required in the formation of the norites, regardless of whether the parental magma was derived from depleted or primitive mantle. This is comparable to estimates based on the major element composition of the norites. If we assume their parental melt before contamination had ~48 wt% SiO_2, similar to a typical picrite (e.g., Larsen and Pedersen, 2000), then 31% contamination by TTG with 68 wt% SiO_2 (average Maniitsoq felsic orthogneiss; Gardiner et al., 2019) is required to produce the 54 wt% average SiO_2 of the norite belt samples.

Source and Parental Melt Composition

As trace elements alone cannot distinguish between a depleted- or primitive-mantle derived melt, we extend this contamination modelling to Hf isotopes to place constraints on the nature of the norite belt source. (**Figure 13D**). We calculate the average εHf of the Maniitsoq region felsic crust at ~3.0 Ga using the average εHf of igneous zircons with U-Pb ages between 2,900 and 3,100 Ma (Gardiner et al., 2019). The analysed zircons are mostly from tonalite samples (n = 9), with three granite samples and one diorite, and yield an average εHf of −2.4 ± 1.7 (2σ). Three different potential Hf isotopic compositions of the source are modelled: a primitive mantle-like source (εHf = 0 at 3.0 Ga); depleted mantle formed at 3.8 Ga, which follows CHUR (Bouvier et al., 2008) evolution from solar system formation until 3.8 Ga, then evolves with depleted mantle $^{176}Lu/^{177}Hf$ of 0.03976 (Fisher and Vervoort, 2018; Spencer et al., 2020) after 3.8 Ga (εHf = +3.0 at 3.0 Ga); and depleted mantle formed at 4.56 Ga, which evolves with $^{176}Lu/^{177}Hf$ of 0.0384 (Griffin et al., 2000) from 4.56 Ga (εHf = +5.1 at 3.0 Ga). Different $^{176}Lu/^{177}Hf$ ratios are used for the two models so that they converge at present day depleted mantle εHf values (Vervoort and Blichert-Toft, 1999). The norite parental magma is assumed to have an NMORB-like Hf/Yb for the two depleted mantle models (Gale et al., 2013), and primitive mantle-like Hf/Yb for the primitive mantle model (Sun and McDonough, 1989), both normalised to the average Yb concentration of the norites and melanorites.

The modelled mixing curves show that no amount of crustal contamination of a melt derived from a primitive mantle-like source can match the average trace element and Hf isotope characteristics of the norite belt samples; contamination of a primitive-mantle derived melt with initial εHf = 0 produces εHf values that are too low at a given La/Yb for all but one sample. By contrast, contamination of 3.8 and 4.56 Ga depleted mantle sources can satisfy the trace element-εHf relationships, and produce εHf in the range observed in the norites and melanorites (εHf = −1.1 to 0.0; excluding outlier samples) with 13–28 and 20–36 wt% crustal contamination, respectively. While the amount of crustal contamination calculated is clearly dependent on the timing of source depletion, the Hf-isotope characteristics of the norites and melanorites are also consistent with high degrees of crustal contamination.

Several other features of the Maniitsoq Norite Belt are consistent with a depleted source. Trace elements not present in high concentrations in local felsic crust suggest a broadly depleted pattern, with primitive mantle normalised Nb < Ti ≈ HREEs (**Figure 7**). Correcting for plagioclase fractionation, Al_2O_3/TiO_2 ratios calculated for the norites and melanorites are high (~50), consistent with formation from a source previously depleted in TiO_2 (Kamber and Tomlinson, 2019). Though this ratio can be modified by assimilation, these calculated values are higher than the average Maniitsoq felsic orthogneiss Al_2O_3/TiO_2 ratio of 39 ± 4 (average of data from Gardiner et al., 2019), suggesting it is a primary feature. Finally, slightly positive εNd values and εHf-trace element characteristics require a depleted source for any amount of crustal contamination. Though the timing of this source depletion is poorly constrained due to high degrees of crustal contamination, relationships between εHf and trace element indicators of crustal contamination are consistent with source depletion occurring 100s of Myrs before the formation of the Maniitsoq Norite Belt, perhaps in the Eoarchaean (Gardiner et al., 2019).

The complex crustal contamination, fractionation and metamorphic processes undergone by the Maniitsoq Norite Belt make it difficult to constrain the nature of its parental magmas. However, inferred crystallising assemblages of orthopyroxene, clinopyroxene, and plagioclase, and compositions which diverge from ~13 wt% MgO (**Figures 4, 5**), suggest that the magma that formed the norites was not particularly ultramafic. The consistently high SiO_2 contents in the norites and melanorites suggests that all samples were crustally contaminated, and that crustal contamination began before the emplacement of the norite magmas. It is therefore possible that the norite belt represents only the upper levels of a magmatic system that had already undergone considerable crustal assimilation and fractional crystallisation. Abundant peridotite bodies in the Maniitsoq region identified during fieldwork are potential candidates for the lower magma chambers in which this assimilation and crystallisation occurred.

TECTONIC INTERPRETATION

The Maniitsoq Norite Belt Did Not Form in Response to a Giant Impact

Garde et al. (2012) and (2013) interpreted the Maniitsoq Norite Belt as a series of post-kinematic intrusions of crustally contaminated ultramafic melts. On the basis of overlapping ages with the youngest components of the Finnefjeld Orthogneiss complex, and superficial similarities to impact melt dykes from Sudbury, Garde et al. (2012) and (2013) suggested they formed in response to a large bolide impact at ~3 Ga, later refined to 3,001 ± 2 Ma (Scherstén and Garde, 2013). This impact was purported to have resulted in the crushing and homogenisation of the regional gneisses, producing the Finnefjeld Orthogneiss Complex, along with complete isotopic resetting of zircon over a wide area (~100 km diameter) due to regional hydrothermal alteration by infiltration of seawater along impact generated fractures (Scherstén and Garde, 2013).

A number of observations presented in this paper directly contradict the interpretations of Garde et al. (2012) and (2013), and are incompatible with an impact model. The norites are not post-kinematic (*Field Observations and Sampling*), and formed during an ongoing period of TTG production, deformation, and metamorphism in the Akia Terrane (*Metamorphism and alteration of the Maniitsoq Norite Belt*). The interpreted emplacement age of the majority of the norite belt (3,013 ± 1 Ma) is significantly older than the 3,001 ± 2 Ma (n = 37) mean age proposed for a giant impact in the Maniitsoq region (Scherstén and Garde, 2013). A Welch's *t*-test gives a probability of these mean ages being identical of 1.7×10^{-13}, meaning we can assert with ≫99% confidence that the norite belt is older than the proposed impact age. Furthermore, the difference in U-Pb zircon age between the Imiak Hill norites and the rest of the belt is inconsistent with an impact event; noritic magmas formed over a period of ~12 Myrs cannot have been generated by a single impact. Finally, we see no evidence for regional hydrothermal alteration seawater in response to an impact, which was suggested to post-date norite intrusion (Scherstén and Garde, 2013). The Maniitsoq Norite Belt is dominated by dry granulite-facies assemblages with low volatile contents (LOI), and limited, localised amphibolite-facies retrogression. Bulk rock $\delta^{18}O$ values above mantle values cannot be explained by seawater infiltration, which, despite uncertainties surrounding the composition of Archaean seawater, would be expected to lower the $\delta^{18}O$ of mantle-derived mafic rocks (Jaffrés et al., 2007; Tartèse et al., 2017). These observations clearly rule out an impact origin for the Maniitsoq Norite Belt (Garde et al., 2012, Garde et al., 2013), and we concur with recent studies suggesting that the Mesoarchaean evolution of the Akia Terrane was not influenced by a giant impact (Steenfelt et al., in review; Reimold et al., 2013; Kirkland et al., 2018; Gardiner et al., 2019; Yakymchuk et al., 2020).

Formation of the Maniitsoq Norite Belt

Based on the constraints outlined in this study, a tectonic model for the formation of the Maniitsoq Norite Belt must satisfy the following observations: 1) essentially synchronous formation of TTGs and norite, with norite intrusion occurring during ongoing TTG production; 2) norite intrusion into hot, thin crust and lithosphere, with low pressure–high temperature granulite-facies metamorphism closely following norite intrusion and contemporaneous with ongoing TTG production; 3) norite formation through extensive crustal contamination of a depleted mantle-derived magma.

Though TTG petrogenesis is largely beyond the scope of this paper, the close temporal and spatial relationships between the Maniitsoq Norite Belt and their host TTGs necessitates some consideration of TTG formation. TTGs are widely understood to form through melting of hydrated mafic rocks (Moyen and Martin, 2012). However, recent work has suggested that TTG parental melts could form through extensive crystallisation of a mafic parental melt (Laurent et al., 2020), raising the possibility that the norites and

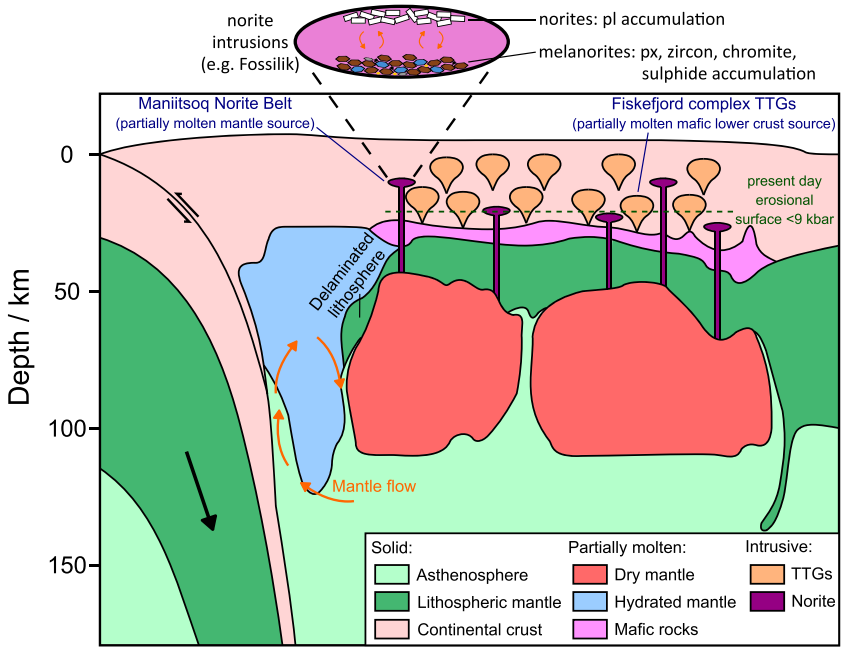

FIGURE 15 | Schematic diagram of synchronous norite and TTG formation in an ultra-hot orogeny, modified from numerical models by Perchuk et al. (2018), with exaggerated vertical scale. Sizes and shapes of crustal blocks, lithospheric mantle, and various zones of partially molten mantle and mafic lower crust are to scale from Perchuk et al. (2018). Relationships in the crust are simplified and not to scale, with TTG production inferred from locations of partially molten new felsic crust in the numerical models, and norite intrusion inferred to occur above zones of partially molten depleted mantle.

TTGs were cogenetic. We rule out this possibility for a number of reasons. Firstly, ~3 Ga TTGs in the northern Akia Terrane require a contribution from older, likely Eoarchaean, mafic crust (Gardiner et al., 2019). Secondly, the initiation of TTG emplacement in the Fiskefjord Complex at ~3,050 Ma (Garde et al., 2000), significantly predates norite belt formation. Thirdly, mass balance suggests that extensive differentiation of a noritic melt (~13 wt% MgO) to a tonalitic parental melt (~2.5 wt% MgO; Laurent et al., 2020), would require the generation of large volumes of mafic cumulates complementary to the voluminous TTGs that host the norites. However, a lack of strong magnetic anomalies in the Fiskefjord Complex is inconsistent with the presence of large volumes of mafic cumulates beneath the norite belt (Steenfelt et al., in review), and norites represent only a minor portion of the exposed crust in the Fiskefjord Complex. We conclude that the close associations between norites and TTGs does not indicate that they were cogenetic, and that synchronous production of TTGs and norites requires a tectonic setting capable of simultaneously producing partial melts of both mafic crust (TTGs) and mantle (norites).

Subduction zones are commonly invoked for formation of TTGs in the Archaean, either through direct melting of subducted oceanic crust (e.g., Hastie et al., 2016), or through melting of thickened arc crust (e.g., Nagel et al., 2012). In this scenario, the norites could potentially be produced through hydrous arc melting or back arc extension. However, the modelled conditions of granulite metamorphism with extremely high temperature gradients (>900°C/GPa; *Metamorphism and alteration of the Maniitsoq Norite Belt*) are inconsistent with significantly thickened crust, as might be expected in a modern-style arc setting. Another possibility, consistent with the requirement of thin crust and lithosphere, is that the norites were produced in an extensional setting, such as a rift or a back arc, and supply of mafic magma combined with elevated geothermal gradients drove melting of pre-existing mafic crust to produce the TTGs. However, this model is inconsistent with the onset of TTG formation predating norite belt emplacement, and the greater proportion of TTGs relative to mafic rocks in the Fiskefjord Complex. Furthermore, an extensional setting cannot account for the deformation contemporaneous with formation of the norite belt and its host TTG orthogneisses (*Field Observations and Sampling*, *Age of the Maniitsoq Norite Belt*). An alternative suggestion, consistent with the observed high thermal gradients in the Akia Terrane, are stagnant lid processes (Yakymchuk et al., 2020). However, it is not clear in this scenario what would "trigger" magmatism and metamorphism in the Akia terrane at ~3 Ga.

Instead, we believe the model that can best satisfy the criteria outlined above is an ultra-hot orogeny (Chardon et al., 2009; **Figure 15**). This model lies somewhere between plate tectonic and stagnant lid processes, in that horizontal convergence is required to drive magmatism and metamorphism, but the crust and lithosphere are extremely weak and lithospheric delamination is an important process. Numerical modelling by Perchuk et al. (2018) demonstrates that for mantle temperatures ~150°C higher than the present day (e.g., Herzberg et al., 2010), convergence between thin blocks of continental lithosphere can produce ultra-hot orogens. In this model, underthrusting of one of the continental blocks is accompanied by delamination of lithospheric mantle and mafic lower crust from the over-riding block. This delamination allows hot partially molten depleted asthenospheric mantle to invade beneath the crust, causing high

crustal temperatures and providing a mechanism for melting of mafic lower crust to produce TTGs. Extensive partial melting of the mantle beneath the ultra-hot orogeny and convective asthenospheric upwelling in response to lithospheric delamination provide a mechanism for producing the mafic magmas that gave rise to the norite belt. The orogenic crust (~30 km thick) and lithosphere (~10 km thick) remains thin due to delamination, mechanical weakness, and thermal erosion, and predicted Moho temperatures are high (~900–1100°C; Perchuk et al., 2018). This provides a mechanism for high temperature–low pressure granulite-facies metamorphism that commenced soon after the norite belt emplacement. High crustal temperatures may have also favoured assimilation of continental crust by the norite belt parental magmas, as crustal temperatures may have been close to the melting point of their host TTGs for 10s of Myrs (Perchuk et al., 2018; Taylor et al., 2020; Yakymchuk et al., 2020). This model is consistent with recent suggestions that TTGs in the Maniitsoq region might be derived from relatively low pressure melting of mafic rocks (Yakymchuk et al., 2020), without requiring over-thickening or subduction of mafic crust (Laurent et al., 2020).

Although previous authors have highlighted the role of crustal contamination in the ~2.7–2.0 Ga norite suite (Barnes, 1989; Bridgwater et al., 1995; Järvinen et al., 2019; Mansur and Barnes, 2020), this model differs substantially in the manner in which the mafic-ultramafic precursors of the norites are generated. Models for younger norites typically invoke melting of highly depleted lithospheric mantle (Hall and Hughes, 1987) or melting of more fertile mantle in a rising mantle plume (Wilson, 2012; Zirakparvar et al., 2019). However, formation of the Maniitsoq Norite Belt during an ongoing period of large-scale TTG production, closely followed by widespread regional granulite metamorphism, is also substantially different to the setting in which younger norites formed. We suggest that coupled norite and TTG formation in Archaean ultra-hot orogenies may represent a mode of norite formation unique to norites older than 2.7 Ga.

CONCLUSIONS

The Maniitsoq Norite Belt comprises two main lithologies: plagioclase-rich "norites" and more mafic and pyroxene-rich "melanorites". Both groups have high Mg#, SiO_2 contents, and low TiO_2 contents relative to amphibolites in the Maniitsoq region, and have trace element patterns featuring depleted HREEs, highly enriched LREEs, and negative anomalies in Nb, Ta, and Ti. Field relationships suggest that the norite belt is younger than the oldest mafic rocks in the region, and may have both intruded and been intruded by TTGs. These field relationships are supported by U-Pb zircon dating, which indicates that the majority of the norite belt formed at 3,013 ± 1 Ma, during the ~3,050–2,990 Ma period of TTG production in the Akia Terrane. However, a statistically resolvable age of 3,001 ± 3 Ma for the Imiak Hill intrusion, and age bracketing from TTG enclaves and sheets, suggests that norite magmatism continued for ~12 Myrs. Mineral assemblages dominated by orthopyroxene, clinopyroxene, plagioclase and hornblendereflect granulite-facies metamorphism at temperatures ~800°C and pressures <9 kbar. These conditions imply high thermal gradients of >900°C/GPa in the Akia Terrane at ~3.0 Ga, and require that crust and lithosphere were thin at the time of norite emplacement. The systematics of many trace elements and possibly Nd-isotopes were disturbed during this metamorphism. Differences in the geochemistry of the norites in the melanorites can be explained by formation from the same parental melt, but with the norites predominantly accumulating plagioclase and the melanorites predominantly accumulating pyroxene. The nature of the parental melt to both groups of rocks is difficult to pinpoint, but appears to have been a broadly mafic (MgO ~ 13 wt%) melt of depleted mantle. This melt was strongly contaminated by ~20–30% assimilation of continental crust, before emplacement and possibly during crystallisation of the norites. High degrees of assimilation were facilitated by intrusion of the norites into crust that was already very hot. The timing of the depletion of the Maniitsoq Norite Belt source is difficult to constrain due to the effects of crustal contamination, but positive εNd values and models of crustal contamination that combine trace elements and Hf-isotopes suggest that the source was depleted significantly (100s of Myrs) before the formation of the Maniitsoq Norite Belt. The synchronous production of TTGs and norite in the Akia Terrane at ~3.0 Ga, closely followed by high temperature, low pressure metamorphism is best explained by formation in an ultra-hot orogeny. Despite sharing crustal contamination as a mechanism for generating noritic compositions with younger norites, synchronous production of TTGs and norite in ultra-hot orogenies may be restricted to norites >2.7 Ga.

DATA AVAILABILITY STATEMENT

All datasets presented in this study are included in the article and the **Supplementary Material**.

AUTHOR CONTRIBUTIONS

PW carried out petrography, Hf-Nd analyses, geochemical modelling, and wrote the manuscript. WH provided petrography and EPMA analyses. JT performed Hf-Nd analyses. JH, CK, CY, NG, and KS carried out fieldwork. JH produced the map. CK and HO carried out zircon U-Pb analyses. CK and CY performed phase equilibrium modelling. DZ analysed O isotopes. PL was the industry contact and provided additional unpublished data and interpretations. KS conceived and supervised the study. All authors provided critical feedback and helped shape the research, analysis and manuscript.

FUNDING

This study was supported by Villum Fonden through grant VKR18978 to K.S. Funding for article fees was supplied by the Ministry of Mineral Resources, Government of Greenland.

ACKNOWLEDGMENTS

This study forms part of the Maniitsoq 1:100,000 map sheet project, a project of the Ministry of Mineral Resources, Government of Greenland, and we thank all members of the project who contributed to fieldwork, sampling and interpretations relevant to this paper, particularly Agnete Steenfelt for constructive discussions on the regional geology of the Akia Terrane. We thank North American Nickel, in particular Patti Tirschmann, Sharon Taylor, Gerry Katchen, and James Sparling, for kindly providing access to samples, data, and internal reports from their exploration work in the Maniitsoq Norite Belt. Carsten Münker is thanked for use of the clean lab and analytical facilities at Universität zu Köln, and for help with the interpretations of Hf-Nd isotopes. We extend additional thanks to Frank Wombacher, Christian Marien, and Eric Hasenstab, who helped with labwork for Hf-Nd isotope chemistry. Ilya Bindeman is thanked for use of the O isotope lab at the University of Oregon, and comments and help with interpretations during the writing of this paper. We thank Oscar Laurent and an reviewer for constructive reviews, and Jean-Louis Vigneresse for editorial handling. This study was supported by Villum Fonden through grant VKR18978 to Kristoffer Szilas.

SUPPLEMENTARY MATERIAL

The Supplementary Material for this article can be found online at: https://www.frontiersin.org/articles/10.3389/feart.2020.562062/full#supplementary-material

REFERENCES

Aarestrup, E., Jørgensen, T. R. C., Armitage, P. E. B., Christiansen, O., and Szilas, K. (in press). The Mesoarchean Amikoq Layered Complex of SW Greenland: Part 1. Constraints on the P-T evolution from igneous, metasomatic and metamorphic amphiboles. *Mineralogical Magazine*. doi:10.1180/mgm.2020.68

Aigner-Torres, M., Blundy, J., Ulmer, P., and Pettke, T. (2007). Laser Ablation ICPMS study of trace element partitioning between plagioclase and basaltic melts: an experimental approach. *Contrib. Mineral. Petrol.* 153, 647–667. doi:10.1007/s00410-006-0168-2

Anders, E., and Grevesse, N. (1989). Abundances of the elements: meteoritic and solar. *Geochem. Cosmochim. Acta* 53, 197–214. doi:10.1016/0016-7037(89)90286-x

Arndt, N., Lesher, C. M., and Barnes, S. J. (2008). *Komatiite*. Cambridge: Cambridge University Press.

Ashwal, L. D. (2010). The temporality of anorthosites. *Can. Mineral.* 48, 711–728. doi:10.3749/canmin.48.4.711

Barnes, S.-J., Naldrett, A. J., and Gorton, M. P. (1985). The origin of the fractionation of platinum-group elements in terrestrial magmas. *Chem. Geol.* 53, 303–323. doi:10.1016/0009-2541(85)90076-2

Barnes, S. J. (1989). Are Bushveld U-type parent magmas boninites or contaminated komatiites? *Contrib. Mineral. Petrol.* 101, 447–457. doi:10.1007/bf00372218

Barnicoat, A. C., and Cartwright, I. (1997). The gabbro-eclogite transformation: an oxygen isotope and petrographic study of west Alpine ophiolites. *J. Metamorph. Geol.* 15, 93–104. doi:10.1111/j.1525-1314.1997.00058.x

Bau, M. (1991). Rare-earth element mobility during hydrothermal and metamorphic fluid-rock interaction and the significance of the oxidation state of europium. *Chem. Geol.* 93, 219–230. doi:10.1016/0009-2541(91)90115-8

Becker, H., Horan, M. F., Walker, R. J., Gao, S., Lorand, J.-P., and Rudnick, R. L. (2006). Highly siderophile element composition of the Earth's primitive upper mantle: constraints from new data on peridotite massifs and xenoliths. *Geochem. Cosmochim. Acta* 70, 4528–4550. doi:10.1016/j.gca.2006.06.004

Bédard, J. H. (2001). Parental magmas of the Nain Plutonic Suite anorthosites and mafic cumulates: a trace element modelling approach. *Contrib. Mineral. Petrol.* 141, 747–771. doi:10.1007/s004100100268

Belousova, E., Griffin, W., O'Reilly, S. Y., and Fisher, N. (2002). Igneous zircon: trace element composition as an indicator of source rock type. *Contrib. Mineral. Petrol.* 143, 602–622. doi:10.1007/s00410-002-0364-7

Berthelsen, A., and Bridgwater, D. (1960). On the field occurrence and petrography of some basic dykes of supposed Pre-cambrian age, from the Souther Sukkertoppen District, Western Greenland. GEUS report file 22176. *Grønlands Geologiske Undersøgelse* 24, 1–41.

Bouvier, A., Vervoort, J. D., and Patchett, P. J. (2008). The Lu-Hf and Sm-Nd isotopic composition of CHUR: constraints from unequilibrated chondrites and implications for the bulk composition of terrestrial planets. *Earth Planet Sci. Lett.* 273, 48–57. doi:10.1016/j.epsl.2008.06.010

Bridgwater, D., Mengel, F., Fryer, B., Wagner, P., and Hansen, S. C. (1995). Early Proterozoic mafic dykes in the North Atlantic and Baltic cratons: field setting and chemistry of distinctive dyke swarms. *Geol. Soc. Spec. Publ.* 95, 193–210. doi:10.1144/gsl.sp.1995.095.01.12

Cawood, P. A., and Hawkesworth, C. J. (2014). Earth's middle age. *Geology* 42, 503–506. doi:10.1130/g35402.1

Chardon, D., Gapais, D., and Cagnard, F. (2009). Flow of ultra-hot orogens: a view from the Precambrian, clues for the Phanerozoic. *Tectonophysics* 477, 105–118. doi:10.1016/j.tecto.2009.03.008

Condie, K. C. (2018). A planet in transition: the onset of plate tectonics on Earth between 3 and 2 Ga? *Geoscience Frontiers* 9, 51–60. doi:10.1016/j.gsf.2016.09.001

Condie, K. C., and O'Neill, C. (2010). The Archean-Proterozoic boundary: 500 MY of tectonic transition in Earth history. *Am. J. Sci.* 310, 775–790. doi:10.2475/09.2010.01

Davies, G., Cawthorn, R. G., Barton, J. M., Jr, and Morton, M. (1980). Parental magma to the Bushveld complex. *Nature* 287, 33–35. doi:10.1038/287033a0

Douce, A. E. P. (1993). Titanium substitution in biotite: an empirical model with applications to thermometry, O_2 and H_2O barometries, and consequences for biotite stability. *Chem. Geol.* 108, 133–162. doi:10.1016/0009-2541(93)90321-9

Dyck, B., Reno, B. L., and Kokfelt, T. F. (2015). The majorqaq belt: a record of neoarchaean orogenesis during final assembly of the North Atlantic Craton, southern West Greenland. *Lithos.* 220–223, 253–271. doi:10.1016/j.lithos.2015.01.024

Eiler, J. M., Schiano, P., Kitchen, N., and Stolper, E. M. (2000). Oxygen-isotope evidence for recycled crust in the sources of mid-ocean-ridge basalts. *Nature* 403, 530–534. doi:10.1038/35000553

Fischer-Gödde, M., Becker, H., and Wombacher, F. (2011). Rhodium, gold and other highly siderophile elements in orogenic peridotites and peridotite xenoliths. *Chem. Geol.* 280, 365–383. doi:10.1016/j.chemgeo.2010.11.024

Fisher, C. M., and Vervoort, J. D. (2018). Using the magmatic record to constrain the growth of continental crust-The Eoarchean zircon Hf record of Greenland. *Earth Planet Sci. Lett.* 488, 79–91. doi:10.1016/j.epsl.2018.01.031

Friend, C., Nutman, A. P., Baadsgaard, H., Kinny, P. D., and Mcgregor, V. R. (1996). Timing of late Archaean terrane assembly, crustal thickening and granite emplacement in the Nuuk region, southern West Greenland. *Earth Planet Sci. Lett.* 142, 353–365. doi:10.1016/0012-821x(96)00118-5

Friend, C. R. L., and Nutman, A. P. (2005). New pieces to the Archaean terrane jigsaw puzzle in the Nuuk region, southern West Greenland: steps in transforming a simple insight into a complex regional tectonothermal model. *J. Geol. Soc.* 162, 147–162. doi:10.1144/0016-764903-161

Friend, C. R. L., and Nutman, A. P. (2019). Tectono-stratigraphic terranes in Archaean gneiss complexes as evidence for plate tectonics: the Nuuk region, southern West Greenland. *Gondwana Res.* 72, 213–237. doi:10.1016/j.gr.2019.03.004

Friend, C. R. L., and Nutman, A. P. (1994). Two Archaean granulite-facies metamorphic events in the Nuuk-Maniitsoq region, southern West

Greenland: correlation with the Saglek block, Labrador. *J. Geol. Soc.* 151, 421–424. doi:10.1144/gsjgs.151.3.0421

Gale, A., Dalton, C. A., Langmuir, C. H., Su, Y., and Schilling, J.-G. (2013). The mean composition of ocean ridge basalts. *Geochem. Geophys. Geosy.* 14, 489–518. doi:10.1029/2012gc004334

Garde, A. A. (2007). A mid-Archaean island arc complex in the eastern Akia terrane, Godthåbsfjord, southern West Greenland. *J. Geol. Soc.* 164, 565–579. doi:10.1144/0016-76492005-107

Garde, A. A., Friend, C. R. L., Nutman, A. R., and Marker, M. (2000). Rapid maturation and stabilisation of middle Archaean continental crust: the Akia terrane, southern West Greenland. *Bull. Geol. Soc. Den.* 47, 1–27.

Garde, A. A. (1997). "Geology of Greenland Survey Bulletin 177," in *Accretion and evolution of an Archaean high-grade grey gneiss—amphibolite complex: the Fiskefjord area, southern West Greenland*. Copenhagen, Denmark: Geological Survey of Denmark and Greenland, Ministry of Environment and Energy.

Garde, A. A., McDonald, I., Dyck, B., and Keulen, N. (2012). Searching for giant, ancient impact structures on Earth: the Mesoarchaean Maniitsoq structure, West Greenland. *Earth Planet Sci. Lett.* 337-338, 197–210. doi:10.1016/j.epsl.2012.04.026

Garde, A. A., Pattison, J., Kokfelt, T. F., Mcdonald, I., and Secher, K. (2013). The norite belt in the Mesoarchaean Maniitsoq structure, southern West Greenland: conduit-type Ni-Cu mineralisation in impact-triggered, mantle-derived intrusions? *Geol. Surv. Den. Greenl. Bull.* 28, 45–48. 10.34194/geusb.v28.4722

Garde, A. A. (1991). Post-kinematic diorite intrusions in Archaean basement rocks around outer Fiskefjord, southern West Greenland. *Bull. Geol. Soc. Den.* 39, 167–177.

Gardiner, N. J., Kirkland, C. L., Hollis, J., Szilas, K., Steenfelt, A., Yakymchuk, C., et al. (2019). Building mesoarchaean crust upon Eoarchaean roots: the Akia terrane, West Greenland. *Contrib. Mineral. Petrol.* 174, 1–19. doi:10.1007/s00410-019-1554-x

Griffin, W. L., Pearson, N. J., Belousova, E., Jackson, S. E., Van Achterbergh, E., O'Reilly, S. Y., et al. (2000). The Hf isotope composition of cratonic mantle: LAM-MC-ICPMS analysis of zircon megacrysts in kimberlites. *Geochem. Cosmochim. Acta* 64, 133–147. doi:10.1016/s0016-7037(99)00343-9

Hall, R. P., and Hughes, D. J. (1993). Early Precambrian crustal development: changing styles of mafic magmatism. *J. Geol. Soc.* 150, 625–635. doi:10.1144/gsjgs.150.4.0625

Hall, R. P., and Hughes, D. J. (1987). Noritic dykes of southern West Greenland: early Proterozoic boninitic magmatism. *Contrib. Mineral. Petrol.* 97, 169–182. doi:10.1007/bf00371237

Hammerli, J., Kemp, A. I. S., and Whitehouse, M. J. (2019). *In situ* trace element and Sm-Nd isotope analysis of accessory minerals in an Eoarchean tonalitic gneiss from Greenland: implications for Hf and Nd isotope decoupling in Earth's ancient rocks. *Chem. Geol.* 524, 394–405. doi:10.1016/j.chemgeo.2019.06.025

Hastie, A. R., Fitton, J. G., Bromiley, G. D., Butler, I. B., and Odling, N. W. A. (2016). The origin of Earth's first continents and the onset of plate tectonics. *Geology* 44, 855–858. doi:10.1130/g38226.1

Hawthorne, F. C., Oberti, R., Harlow, G. E., Maresch, W. V., Martin, R. F., Schumacher, J. C., et al. (2012). Nomenclature of the amphibole supergroup. *Am. Mineral.* 97, 2031–2048. doi:10.2138/am.2012.4276

He, H. L., Song, X. Y., Zhai, M. G., Yu, S. Y., and Du, Z. S. (2019). Lower crustal contribution to the magma formation of the Damiao massif-type anorthosite, North China Craton: evidence from zircon Hf-O isotopes. *Precambrian Res.* 332, 105396. doi:10.1016/j.precamres.2019.105396

Herzberg, C., Condie, K., and Korenaga, J. (2010). Thermal history of the Earth and its petrological expression. *Earth Planet Sci. Lett.* 292, 79–88. doi:10.1016/j.epsl.2010.01.022

Hiess, J., Bennett, V. C., Nutman, A. P., and Williams, I. S. (2009). *In situ* U-Pb, O and Hf isotopic compositions of zircon and olivine from Eoarchaean rocks, West Greenland: new insights to making old crust. *Geochim. Cosmochim. Acta* 73, 4489–4516. 10.1016/j.gca.2009.04.019

Hofmann, A. W. (1988). Chemical differentiation of the Earth: the relationship between mantle, continental crust, and oceanic crust. *Earth Planet Sci. Lett.* 90, 297–314. doi:10.1016/0012-821x(88)90132-x

Holness, M. B. (2006). Melt-solid dihedral angles of common minerals in natural rocks. *J. Petrol.* 47, 791–800. doi:10.1093/petrology/egi094

Ickert, R. B. (2013). Algorithms for estimating uncertainties in initial radiogenic isotope ratios and model ages. *Chem. Geol.* 340, 131–138. doi:10.1016/j.chemgeo.2013.01.001

Jaffrés, J. B. D., Shields, G. A., and Wallmann, K. (2007). The oxygen isotope evolution of seawater: a critical review of a long-standing controversy and an improved geological water cycle model for the past 3.4 billion years. *Earth Sci. Rev.* 83, 83–122. doi:10.1016/j.earscirev.2007.04.002

Jaques, A. L. (1981). Petrology and petrogenesis of cumulate peridotites and gabbros from the marum ophiolite complex, Northern Papua New Guinea. *J. Petrol.* 22, 1–40. doi:10.1093/petrology/22.1.1

Järvinen, V., Halkoaho, T., Konnunaho, J., Heinonen, J. S., and Rämö, O. T. (2019). Parental magma, magmatic stratigraphy, and reef-type PGE enrichment of the 2.44-Ga mafic-ultramafic Näränkävaara layered intrusion, Northern Finland. *Miner. Depos.* doi:10.1007/s00126-019-00934-z

Kamber, B. S., and Tomlinson, E. L. (2019). Petrological, mineralogical and geochemical peculiarities of Archaean cratons. *Chem. Geol.* 511, 123–151. doi:10.1016/j.chemgeo.2019.02.011

Kirkland, C. L., Olierook, H., Yakymchuk, C., Gardiner, N. J., Szilas, K., and Johnson, T. (in review). Theoretical versus empirical secular change in Archean zircon composition.

Kirkland, C. L., Smithies, R. H., Taylor, R. J. M., Evans, N., and Mcdonald, B. (2015). Zircon Th/U ratios in magmatic environs. *Lithos* 212–215, 397–414. doi:10.1016/j.lithos.2014.11.021

Kirkland, C. L., Yakymchuk, C., Gardiner, N. J., Szilas, K., Hollis, J., Olierook, H., et al. (2020). Titanite petrochronology linked to phase equilibrium modelling constrains tectono-thermal events in the Akia Terrane, West Greenland. *Chem. Geol.* 536, 119467. doi:10.1016/j.chemgeo.2020.119467

Kirkland, C. L., Yakymchuk, C., Hollis, J., Heide-Jørgensen, H., and Danišík, M. (2018). Mesoarchean exhumation of the Akia terrane and a common Neoarchean tectonothermal history for West Greenland. *Precambrian Res.* 314, 129–144. doi:10.1016/j.precamres.2018.06.004

Larsen, L. M., and Pedersen, A. K. (2000). Processes in high-Mg, high-T magmas: evidence from olivine, chromite and glass in Palaeogene picrites from West Greenland. *J. Petrol.* 41, 1071–1098. doi:10.1093/petrology/41.7.1071

Laurent, O., Björnsen, J., Wotzlaw, J.-F., Bretscher, S., Pimenta Silva, M., Moyen, J.-F., et al. (2020). Earth's earliest granitoids are crystal-rich magma reservoirs tapped by silicic eruptions. *Nat. Geosci.* 13, 163–169. doi:10.1038/s41561-019-0520-6

Le Maitre, R. W., Streckeisen, A., and Zanettin, B. (2002). "Classification and nomenclature." in *Igneous rocks*. (Editor) R. W. Le Maitre Cambridge, United Kingdom: Cambridge University Press, 3–42.

Lightfoot, P. C. (2017). *Nickel sulfide ores and impact melts origin of the Sudbury igneous complex*. Amsterdam: Elsevier.

Lindsley, D. H., and Andersen, D. J. (1983). A two-pyroxene thermometer. *J. Geophys. Res.Solid Earth* 88, A887–A906. doi:10.1029/JB088iS02p0A887

Locock, A. J. (2014). An Excel spreadsheet to classify chemical analyses of amphiboles following the IMA 2012 recommendations. *Comp. Geosc.* 62, 1–11. doi:10.1016/j.cageo.2013.09.011

Longhi, J., Wooden, J., and Coppinger, K. D. (1983). The petrology of high-Mg dykes from the Beartooth Mountains, Montana: a search for the parent magma of the Stillwater Complex. *J. Geophys. Res. Solid Earth*, 88, B53–B69. doi:10.1029/JB088iS01p00B53

Ludwig, K. R. (2012). User 's manual for Isoplot, v3.75, *A geochronological toolkit for microsoft excel*. Berkeley Geochronology Center Special Publications.

Lugmair, G. W., and Marti, K. (1978). Lunar initial 143Nd/144Nd: differential evolution of the lunar crust and mantle. *Earth Planet Sci. Lett.* 39, 349–357. doi:10.1016/0012-821x(78)90021-3

Lyell, C. (1830). *Principles of geology, being an attempt to explain the former changes of the earth's surface, by reference to causes now in operation*. London, United Kingdom: John Murray.

Mansur, E. T., and Barnes, S.-J. (2020). Concentrations of Te, as, Bi, Sb and Se in the marginal zone of the bushveld complex: evidence for crustal contamination and the nature of the magma that formed the merensky reef. *Lithos* 358-359, 105407. doi:10.1016/j.lithos.2020.105407

McDonough, W. F., and Sun, S.-S. (1995). The composition of the Earth. *Chem. Geol.* 120, 223–253. doi:10.1016/0009-2541(94)00140-4

Moyen, J. F., and Martin, H. (2012). Forty years of TTG research. *Lithos* 148, 312–336. doi:10.1016/j.lithos.2012.06.010

Nagel, T. J., Hoffmann, J. E., and Münker, C. (2012). Generation of Eoarchean tonalite-trondhjemite-granodiorite series from thickened mafic arc crust. *Geology* 40, 375–378. doi:10.1130/g32729.1

Næraa, T., Kemp, A. I. S., Scherstén, A., Rehnström, E. F., Rosing, M. T., and Whitehouse, M. J. (2014). A lower crustal mafic source for the ca. 2550Ma Qôrqut Granite Complex in southern West Greenland. *Lithos* 192–195, 291–304. doi:10.1016/j.lithos.2014.02.013

Nguyen, D. K., Morishita, T., Soda, Y., Tamura, A., Ghosh, B., Harigane, Y., et al. (2018). Occurrence of felsic rocks in oceanic gabbros from iodp hole 1473a: implications for evolved melt migration in the lower oceanic crust. *Minerals* 8, 1–30. doi:10.3390/min8120583

Nicholls, J., and Russell, J. K. (2016). Igneous rock associations 20. Pearce element ratio diagrams: linking geochemical data to magmatic processes. *Geoscience Canada* 43, 133–146. doi:10.12789/geocanj.2016.43.095

Nielsen, S. G., Baker, J. A., and Krogstad, E. J. (2002). Petrogenesis of an early Archaean (3.4 Ga) norite dyke, Isua, West Greenland: evidence for early Archaean crustal recycling? *Precambrian Res.* 118, 133–148. doi:10.1016/s0301-9268(02)00108-0

Nutman, A. P., Friend, C. R. L., Barker, S. L. L., and McGregor, V. R. (2004). Inventory and assessment of Palaeoarchaean gneiss terrains and detrital zircons in southern West Greenland. *Precambrian Res.* 135, 281–314. doi:10.1016/j.precamres.2004.09.002

Nutman, A. P., Friend, C. R. L., and Hiess, J. (2010). Setting of the 2560 Ma qorqut granite complex in the archean crustal evolution of southern West Greenland. *Am. J. Sci.* 310, 1081–1114. doi:10.2475/09.2010.12

Nutman, A. P., Hagiya, H., and Maruyama, S. (1995). SHRIMP U-Pb single zircon geochronology of a Proterozoic mafic dyke, Isukasia, southern West Greenland. *Bull. Geol. Soc. Den.* 42, 17–22.

Pagé, P., and Barnes, S.-J. (2016). The influence of chromite on osmium, iridium, ruthenium and rhodium distribution during early magmatic processes. *Chem. Geol.* 420, 51–68. doi:10.1016/j.chemgeo.2015.11.002

Pearce, J. A. (2008). Geochemical fingerprinting of oceanic basalts with applications to ophiolite classification and the search for Archean oceanic crust. *Lithos* 100, 14–48. doi:10.1016/j.lithos.2007.06.016

Pearce, J. A., and Reagan, M. K. (2019). Identification, classification, and interpretation of boninites from Anthropocene to Eoarchean using Si-Mg-Ti systematics data manipulation before classification. *Geosphere* 15, 1–30. doi:10.1130/ges01661.1

Pearce, T. H. (1968). A contribution to the theory of variation diagrams. *Contrib. Mineral. Petrol.* 19, 142–157. doi:10.1007/bf00635485

Perchuk, A. L., Safonov, O. G., Smit, C. A., van Reenen, D. D., Zakharov, V. S., and Gerya, T. V. (2018). Precambrian ultra-hot orogenic factory: making and reworking of continental crust. *Tectonophysics* 746, 572–586. doi:10.1016/j.tecto.2016.11.041

Ravenelle, J. F., Weiershauser, L., and Cole, G. (2017). Report No.: 3CN024.004. Updated Independent Technical Report for the Maniitsoq Nickel-Copper-Cobalt-PGM Project, Greenland. Available at: https://s1.q4cdn.com/725069486/files/doc_downloads/technical_reports/Technical_Report_2017.pdf (Accessed March 17, 2017).

Reimold, W. U., Gibson, R. L., and Koeberl, C. (2013). Comment on "Searching for giant, ancient impact structures on Earth: the Mesoarchaean Maniitsoq structure, West Greenland" by Garde et al. *Earth Planet. Sci. Lett.* 369–370, 333–335. doi:10.1016/j.epsl.2013.04.014

Riciputi, L. R., Valley, J. W., and McGregor, V. R. (1990). Conditions of Archean granulite metamorphism in the Godthab-Fiskenaesset region, southern West Greenland. *J. Metamorph. Geol.* 8, 171–190. doi:10.1111/j.1525-1314.1990.tb00464.x

Russell, J. K., Nicholls, J., Stanley, C. R., and Pearce, T. H. (1990). Pearce element ratios: a paradigm for testing hypotheses. *Eos.* 71, 234–247. doi:10.1029/eo071i005p00234

Sambridge, M., and Lambert, D. D. (1997). Propagating errors in decay equations: examples from the Re-Os isotopic system. *Geochem. Cosmochim. Acta* 61, 3019–3024. doi:10.1016/s0016-7037(97)00130-0

Sandiford, M., and Powell, R. (1991). Some remarks on high-temperature—low-pressure metamorphism in convergent orogens. *J. Metamorph. Geol.* 9, 333–340. doi:10.1111/j.1525-1314.1991.tb00527.x

Scherstén, A., and Garde, A. A. (2013). Complete hydrothermal re-equilibration of zircon in the Maniitsoq structure, West Greenland: a 3001 Ma minimum age of impact? *Meteorit. Planet. Sci.* 48, 1472–1498. doi:10.1111/maps.12169

Secher, K. (2001). Geological Survey of Denmark and Greenland Report 2001/123: the Pd + Pt dispersion in noritic and undifferentiated mafic rocks of the Archaean craton east of Maniitsoq, southern West Greenland. Copenhagen, Denmark: Geological Survey of Denmark and Greenland Bulletin.

Secher, K. (1983). The Geological Survey of Greenland Report No. 115: noritic rocks and associated nickel-copper-sulphide occurences in Sukkertoppen district, central West Greenland. Copenhagen, Denmark: Geological Survey of Denmark and Greenland Bulletin.

Smithies, R. H., Champion, D. C., and Sun, S.-S. (2004). The case for Archaean boninites. *Contrib. Mineral. Petrol.* 147, 705–721. doi:10.1007/s00410-004-0579-x

Söderlund, U., Patchett, P. J., Vervoort, J. D., and Isachsen, C. E. (2004). The 176Lu decay constant determined by Lu-Hf and U-Pb isotope systematics of Precambrian mafic intrusions. *Earth Planet Sci. Lett.* 219, 311–324. doi:10.1016/s0012-821x(04)00012-3

Spencer, C. J., Kirkland, C. L., Roberts, N. M. W., Evans, N. J., and Liebmann, J. (2020). Strategies towards robust interpretations of *in situ* zircon Lu–Hf isotope analyses. *Geoscience Front* 11, 843–853. doi:10.1016/j.gsf.2019.09.004

Srivastava, R. K. (2008). Global intracratonic boninite-Norite magmatism during the neoarchean-Paleoproterozoic: evidence from the central Indian bastar Craton. *Int. Geol. Rev.* 50, 61–74. doi:10.2747/0020-6814.50.1.61

Steenfelt, A., Hollis, J. A., Kirkland, C. L., Olierook, H., Szilas, K., Yakymchuk, C., and Gardiner, N. J. (in review). New Meso- and Neoarchaean crustal components in the Akia terrane, southern West Greenland: spatial analysis of aeromagnetic, lithological, geochemical and zircon U-Pb isotope data. *Precambrian Research*.

Sun, S. -s., and McDonough, W. F. (1989). Chemical and isotopic systematics of oceanic basalts: implications for mantle composition and processes. *Geol. Soc. Spec. Pub* 42, 313–345. doi:10.1144/gsl.sp.1989.042.01.19

Szilas, K., Kelemen, P. B., and Bernstein, S. (2015). Peridotite enclaves hosted by Mesoarchaean TTG-suite orthogneisses in the Fiskefjord region of southern West Greenland. *Georesj.* 7, 22–34. doi:10.1016/j.grj.2015.03.003

Szilas, K., Tusch, J., Hoffmann, J. E., Garde, A. A., and Münker, C. (2017). "Hafnium isotope constraints on the origin of mesoarchaean andesites in southern West Greenland, North Atlantic Craton." in *Crust–mantle interactions and granitoid diversification: insights from archaean cratons*. London, UK: Geological Society of London, 449.

Szilas, K., van Hinsberg, V., McDonald, I., Næraa, T., Rollinson, H., Adetunji, J., et al. (2018). Highly refractory Archaean peridotite cumulates: petrology and geochemistry of the seqi ultramafic complex, SW Greenland. *Geoscience Front* 9, 689–714. 10.1016/j.gsf.2017.05.003

Tartèse, R., Chaussidon, M., Gurenko, A., Delarue, F., and Robert, F. (2017). Warm Archaean oceans reconstructed from oxygen isotope composition of early-life remnants. *Geochem. Persp. Let* 3, 55–65. doi:10.7185/geochemlet.1706

Taylor, R. J. M., Johnson, T. E., Clark, C., and Harrison, R. J. (2020). Persistence of melt-bearing Archean lower crust for >200 m.y.-an example from the Lewisian complex, northwest Scotland. *Geology* 48, 221–225. doi:10.1130/g46834.1

Vervoort, J. D., and Blichert-Toft, J. (1999). Evolution of the depleted mantle: Hf isotope evidence from juvenile rocks through time. *Geochem. Cosmochim. Acta* 63, 533–556. doi:10.1016/s0016-7037(98)00274-9

Vervoort, J. D., Plank, T., and Prytulak, J. (2011). The Hf-Nd isotopic composition of marine sediments. *Geochem. Cosmochimica Acta* 75, 5903–5926. doi:10.1016/j.gca.2011.07.046

Vezinet, A., Pearson, D. G., Thomassot, E., Stern, R. A., Sarkar, C., Luo, Y., Fisher, C. M., et al. (2018). Hydrothermally-altered mafic crust as source for early Earth TTG: Pb/Hf/O isotope and trace element evidence in zircon from TTG of the Eoarchean Saglek Block, N. Labrador, *Earth Planet Sci. Lett.* 503, 95–107. doi:10.1016/j.epsl.2018.09.015

Whalen, J. B., Percival, J. A., McNicoll, V. J., and Longstaffe, F. J. (2002). A mainly crustal origin for tonalitic granitoid rocks, superior province, Canada: implications for late Archean tectonomagmatic processes. *J. Petrol.* 43, 1551–1570. doi:10.1093/petrology/43.8.1551

Wilson, A. H. (2012). A chill sequence to the bushveld complex: insight into the first stage of emplacement and implications for the parental magmas. *J. Petrol.* 53, 1123–1168. doi:10.1093/petrology/egs011

Wittig, N., Webb, M., Pearson, D. G., Dale, C. W., Ottley, C. J., Hutchison, M., et al. (2010). Formation of the North Atlantic Craton: timing and mechanisms constrained from Re-Os isotope and PGE data of peridotite xenoliths from S.W. Greenland. *Chem. Geol.* 276, 166–187. 10.1016/j.chemgeo.2010.06.002

Yakymchuk, C., Hinsberg, V., van, Kirkland, C., Szilas, K., Kinney, C., Kendrick, J., and Hollis, J. (in review). Metasomatic ruby growth during the final stages of cratonization, Maniitsoq region, southern West Greenland. Contributions to Mineralogy and Petrology.

Yakymchuk, C., Kirkland, C. L., and Clark, C. (2018). Th/U ratios in metamorphic zircon. *J. Metamorph. Geol.* 36, 715–737. doi:10.1111/jmg.12307

Yakymchuk, C., Kirkland, C. L., Hollis, J. A., Kendrick, J., Gardiner, N. J., and Szilas, K. (2020). Mesoarchean partial melting of mafic crust and tonalite production during high-T–low-P stagnant tectonism, Akia Terrane, West Greenland. *Precambrian Res.* 339, 105615. doi:10.1016/j.precamres.2020.105615

Yi, K., Bennett, V. C., Nutman, A. P., and Lee, S. R. (2014). Tracing Archaean terranes under Greenland's Icecap: U-Th-Pb-Hf isotopic study of zircons from melt-water rivers in the Isua area. *Precambrian Res.* 255, 900–921. doi:10.1016/j.precamres.2014.04.006

Zhao, Z.-F., and Zheng, Y.-F. (2003). Calculation of oxygen isotope fractionation in magmatic rocks. *Chem. Geol.* 193, 59–80. doi:10.1016/s0009-2541(02)00226-7

Zirakparvar, N. A., Mathez, E. A., Rajesh, H. M., and Choe, S. (2019). Lu-Hf isotopic evidence of a deep mantle plume source for the ~2.06 Ga Bushveld large igneous province. *Lithos* 348–349, 105168. doi:10.1016/j.lithos.2019.105168

Conflict of Interest: Author PL was employed by the company North American Nickel Inc.

The remaining authors declare that the research was conducted in the absence of any commercial or financial relationships that could be construed as a potential conflict of interest.